

Shape Quantization and Recognition with Randomized Trees

Yali Amit

Department of Statistics, University of Chicago, Chicago, IL, 60637, U.S.A.

Donald Geman

*Department of Mathematics and Statistics, University of Massachusetts,
Amherst, MA 01003, U.S.A.*

We explore a new approach to shape recognition based on a virtually infinite family of binary features (queries) of the image data, designed to accommodate prior information about shape invariance and regularity. Each query corresponds to a spatial arrangement of several local topographic codes (or tags), which are in themselves too primitive and common to be informative about shape. All the discriminating power derives from relative angles and distances among the tags. The important attributes of the queries are a natural *partial ordering* corresponding to increasing structure and complexity; *semi-invariance*, meaning that most shapes of a given class will answer the same way to two queries that are successive in the ordering; and *stability*, since the queries are not based on distinguished points and substructures.

No classifier based on the full feature set can be evaluated, and it is impossible to determine a priori which arrangements are informative. Our approach is to select informative features and build tree classifiers at the same time by inductive learning. In effect, each tree provides an approximation to the full posterior where the features chosen depend on the branch that is traversed. Due to the number and nature of the queries, standard decision tree construction based on a fixed-length feature vector is not feasible. Instead we entertain only a small random sample of queries at each node, constrain their complexity to increase with tree depth, and grow multiple trees. The terminal nodes are labeled by estimates of the corresponding posterior distribution over shape classes. An image is classified by sending it down every tree and aggregating the resulting distributions.

The method is applied to classifying handwritten digits and synthetic linear and nonlinear deformations of three hundred \LaTeX symbols. State-of-the-art error rates are achieved on the National Institute of Standards and Technology database of digits. The principal goal of the experiments on \LaTeX symbols is to analyze invariance, generalization error and related issues, and a comparison with artificial neural networks methods is presented in this context.

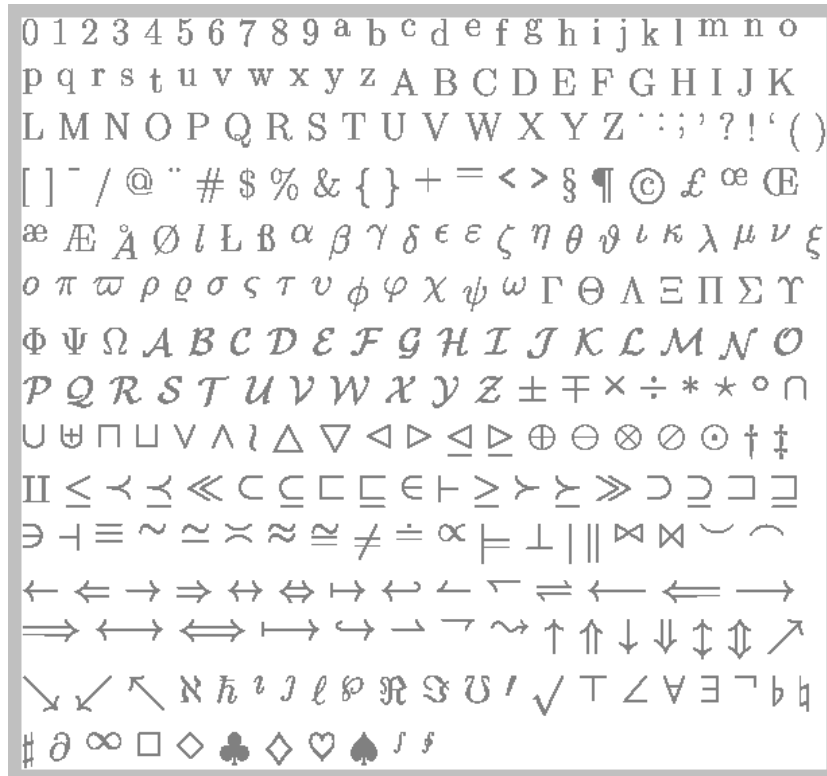


Figure 1: \LaTeX symbols.

1 Introduction

We explore a new approach to shape recognition based on the joint induction of shape features and tree classifiers. The data are binary images of two-dimensional shapes of varying sizes. The number of shape classes may reach into the hundreds (see Figure 1), and there may be considerable within-class variation, as with handwritten digits. The fundamental problem is how to design a practical classification algorithm that incorporates the prior knowledge that the shape classes remain invariant under certain transformations. The proposed framework is analyzed within the context of invariance, generalization error, and other methods based on inductive learning, principally artificial neural networks (ANN).

Classification is based on a large, in fact virtually infinite, family of binary

features of the image data that are constructed from local topographic codes ("tags"). A large sample of small subimages of fixed size is recursively partitioned based on individual pixel values. The tags are simply labels for the cells of each successive partition, and each pixel in the image is assigned all the labels of the subimage centered there. As a result, the tags do not involve detecting distinguished points along curves, special topological structures, or any other complex attributes whose very definition can be problematic due to locally ambiguous data. In fact, the tags are too primitive and numerous to classify the shapes.

Although the mere existence of a tag conveys very little information, one can begin discriminating among shape classes by investigating just a few spatial relationships among the tags, for example, asking whether there is a tag of one type "north" of a tag of another type. Relationships are specified by coarse constraints on the angles of the vectors connecting pairs of tags and on the relative distances among triples of tags. No absolute location or scale constraints are involved. An image may contain one or more instances of an arrangement, with significant variations in location, distances, angles, and so forth. There is one binary feature ("query") for each such spatial arrangement; the response is positive if a collection of tags consistent with the associated constraints is present anywhere in the image. Hence a query involves an extensive disjunction (ORing) operation.

Two images that answer the same to every query must have very similar shapes. In fact, it is reasonable to assume that the shape class is determined by the full feature set; that is, the theoretical Bayes error rate is zero. But no classifier based on the full feature set can be evaluated, and it is impossible to determine a priori which arrangements are informative. Our approach is to select informative features and build tree classifiers (Breiman, Friedman, Olshen, & Stone, 1984; Casey & Nagy, 1984; Quinlan, 1986) *at the same time* by inductive learning. In effect, each tree provides an approximation to the full posterior where the features chosen depend on the branch that is traversed.

There is a natural partial ordering on the queries that results from regarding each tag arrangement as a labeled graph, with vertex labels corresponding to the tag types and edge labels to angle and distance constraints (see Figures 6 and 7). In this way, the features are ordered according to increasing structure and complexity. A related attribute is *semi-invariance*, which means that a large fraction of those images of a given class that answer the same way to a given query will also answer the same way to any query immediately succeeding it in the ordering. This leads to nearly invariant classification with respect to many of the transformations that preserve shape, such as scaling, translation, skew and small, nonlinear deformations of the type shown in Figure 2.

Due to the partial ordering, tree construction with an infinite-dimensional feature set is computationally efficient. During training, multiple trees (Breiman, 1994; Dietterich & Bakiri, 1995; Shlien, 1990) are grown, and a

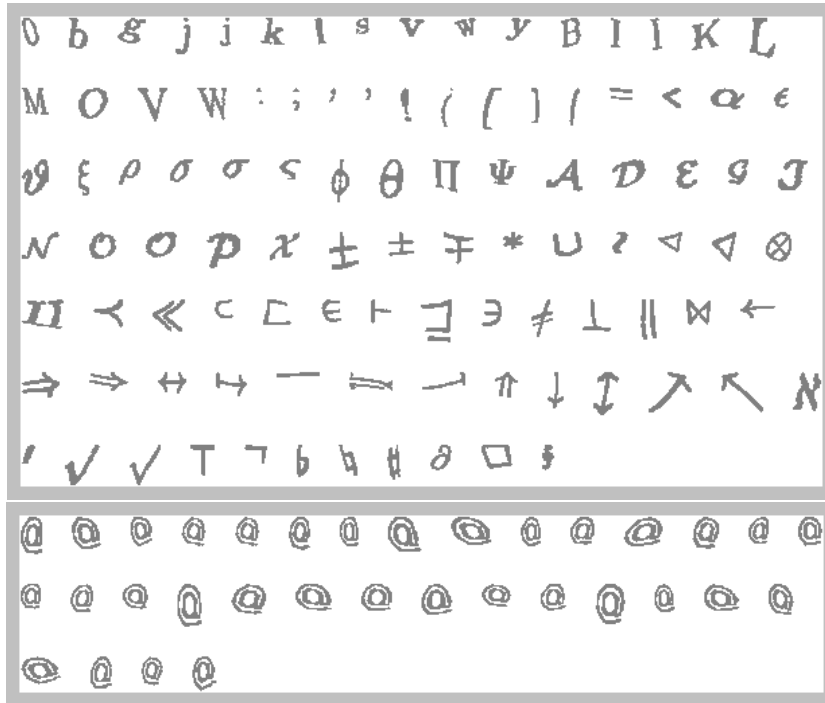


Figure 2: (Top) Perturbed \LaTeX symbols. (Bottom) Training data for one symbol.

form of randomization is used to reduce the statistical dependence from tree to tree; weak dependence is verified experimentally. Simple queries are used at the top of the trees, and the complexity of the queries increases with tree depth. In this way semi-invariance is exploited, and the space of shapes is systematically explored by calculating only a tiny fraction of the answers.

Each tree is regarded as a random variable on image space whose values are the terminal nodes. In order to recognize shapes, each terminal node of each tree is labeled by an estimate of the conditional distribution over the shape classes given that an image reaches that terminal node. The estimates are simply relative frequencies based on training data and require no optimization. A new data point is classified by dropping it down each of the trees, averaging over the resulting terminal distributions, and taking the mode of this aggregate distribution. Due to averaging and weak dependence, considerable errors in these estimates can be tolerated. Moreover, since tree-growing (i.e., question selection) and parameter estimation can be separated, the estimates can be refined indefinitely *without reconstruct-*

ing the trees, simply by updating a counter in each tree for each new data point.

The separation between tree making and parameter estimation, and the possibility of using different training samples for each phase, opens the way to selecting the queries based on either unlabeled samples (i.e., unsupervised learning) or samples from only some of the shape classes. Both of these perform surprisingly well compared with ordinary supervised learning.

Our recognition strategy differs from those based on true invariants (algebraic, differential, etc.) or structural features (holes, endings, etc.). These methods certainly introduce prior knowledge about shape and structure, and we share that emphasis. However, invariant features usually require image normalization or boundary extraction, or both, and are generally sensitive to shape distortion and image degradation. Similarly, structural features can be difficult to express as well-defined functions of the image (as opposed to model) data. In contrast, our queries are stable and primitive, precisely because they are not truly invariant and are not based on distinguished points or substructures.

A popular approach to multiclass learning problems in pattern recognition is based on ANNs, such as feedforward, multilayer perceptrons (Dietterich & Bakiri, 1995; Fukushima & Miyake, 1982; Knerr, Personnaz, & Dreyfus, 1992; Martin & Pitman, 1991). For example, the best rates on handwritten digits are reported in LeCun et al. (1990). Classification trees and neural networks certainly have aspects in common; for example, both rely on training data, are fast online, and require little storage (see Brown, Corruble, & Pittard, 1993; Gelfand & Delp, 1991). However, our approach to invariance and generalization is, by comparison, more direct in that certain properties are acquired by hardwiring rather than depending on learning or image normalization. With ANNs, the emphasis is on parallel and local processing and a limited degree of disjunction, in large part due to assumptions regarding the operation of the visual system. However, only a limited degree of invariance can be achieved with such models. In contrast, the features here involve extensive disjunction and more global processing, thus achieving a greater degree of invariance. This comparison is pursued in section 12.

The article is organized as follows. Other approaches to invariant shape recognition are reviewed in section 2; synthesized random deformations of 293 basic L^AT_EX symbols (see Figures 1 and 2) provide a controlled experimental setting for an empirical analysis of invariance in a high-dimensional shape space. The basic building blocks of the algorithm, namely the tags and the tag arrangements, are described in section 3. In section 4 we address the fundamental question of how to exploit the discriminating power of the feature set; we attempt to motivate the use of multiple decision trees in the context of the ideal Bayes classifier and the trade-off between approximation error and estimation error. In section 5 we explain the roles

of the partial ordering and randomization for both supervised and unsupervised tree construction; we also discuss and quantify semi-invariance. Multiple decision trees and the full classification algorithm are presented in section 6, together with an analysis of the dependence on the training set. In section 7 we calculate some rough performance bounds, for both individual and multiple trees. Generalization experiments, where the training and test samples represent different populations, are presented in section 8, and incremental learning is addressed in section 9. Fast indexing, another possible role for shape quantization, is considered in section 10. We then apply the method in section 11 to a real problem—classifying handwritten digits—using the National Institute of Standards and Technology (NIST) database for training and testing, achieving state-of-the-art error rates. In section 12 we develop the comparison with ANNs in terms of invariance, generalization error, and connections to observed functions in the visual system. We conclude in section 13 by assessing extensions to other visual recognition problems.

2 Invariant Recognition

Invariance is perhaps the fundamental issue in shape recognition, at least for isolated shapes. Some basic approaches are reviewed within the following framework. Let \mathbf{X} denote a space of digital images, and let \mathcal{C} denote a set of shape classes. Let us assume that each image $\mathbf{x} \in \mathbf{X}$ has a true class label $Y(\mathbf{x}) \in \mathcal{C} = \{1, 2, \dots, K\}$. Of course, we cannot directly observe Y . In addition, there is a probability distribution P on \mathbf{X} . Our goal is to construct a classifier $\hat{Y}: \mathbf{X} \rightarrow \mathcal{C}$ such that $P(\hat{Y} \neq Y)$ is small.

In the literature on statistical pattern recognition, it is common to address some variation by preprocessing or normalization. Given \mathbf{x} , and before estimating the shape class, one estimates a transformation ψ such that $\psi(\mathbf{x})$ represents a standardized image. Finding ψ involves a sequence of procedures that brings all images to the same size and then corrects for translation, slant, and rotation by one of a variety of methods. There may also be some morphological operations to standardize stroke thickness (Bottou et al., 1994; Hastie, Buja, & Tibshirani, 1995). The resulting image is then classified by one of the standard procedures (discriminant analysis, multilayer neural network, nearest neighbors, etc.), in some cases essentially ignoring the global spatial properties of shape classes. Difficulties in generalization are often encountered because the normalization is not robust or does not accommodate nonlinear deformations. This deficiency can be ameliorated only with very large training sets (see the discussions in Hussain & Kabuka, 1994; Raudys & Jain, 1991; Simard, LeCun, & Denker, 1994; Werbos, 1991, in the context of neural networks). Still, it is clear that robust normalization

methods which reduce variability and yet preserve information can lead to improved performance of any classifier; we shall see an example of this in regard to slant correction for handwritten digits.

Template matching is another approach. One estimates a transformation from \mathbf{x} for each of the prototypes in the library. Classification is then based on the collection of estimated transformations. This requires explicit modeling of the prototypes and extensive computation at the estimation stage (usually involving relaxation methods) and appears impractical with large numbers of shape classes.

A third approach, closer in spirit to ours, is to search for invariant functions $\Phi(\mathbf{x})$, meaning that $P(\Phi(\mathbf{x}) = \phi_c | Y = c) = 1$ for some constants ϕ_c , $c = 1, \dots, K$. The discriminating power of Φ depends on the extent to which the values ϕ_c are distinct. Many invariants for planar objects (based on single views) and nonplanar objects (based on multiple views) have been discovered and proposed for recognition (see Reiss, 1993, and the references therein). Some invariants are based on Fourier descriptors and image moments; for example, the magnitude of Zernike moments (Khotanzad & Lu, 1991) is invariant to rotation. Most invariants require computing tangents from estimates of the shape boundaries (Forsyth et al., 1991; Sabourin & Mitiche, 1992). Examples of such invariants include inflexions and discontinuities in curvature. In general, the mathematical level of this work is advanced, borrowing ideas from projective, algebraic, and differential geometry (Mundy & Zisserman, 1992).

Other successful treatments of invariance include geometric hashing (Lamdan, Schwartz, & Wolfson, 1988) and nearest-neighbor classifiers based on affine invariant metrics (Simard et al., 1994). Similarly, structural features involving topological shape attributes (such as junctions, endings, and loops) or distinguished boundary points (such as points of high curvature) have some invariance properties, and many authors (e.g., Lee, Srihari, & Gaborski, 1991) report much better results with such features than with standardized raw data.

In our view, true invariant features of the form above might not be sufficiently stable for intensity-based recognition because the data structures are often too crude to analyze with continuum-based methods. In particular, such features are not invariant to nonlinear deformations and depend heavily on preprocessing steps such as normalization and boundary extraction. Unless the data are of very high quality, these steps may result in a lack of robustness to distortions of the shapes, due, for example, to digitization, noise, blur, and other degrading factors (see the discussion in Reiss, 1993). Structural features are difficult to model and to extract from the data in a stable fashion. Indeed, it may be more difficult to recognize a "hole" than to recognize an "8." (Similar doubts about hand-crafted features and distinguished points are expressed in Jung & Nagy, 1995.) In addition, if one could recognize the components of objects without recognizing the objects themselves, then the choice of classifier would likely be secondary.

Our features are not invariant. However, they are semi-invariant in an appropriate sense and might be regarded as coarse substitutes for some of the true geometric, point-based invariants in the literature already cited. In this sense, we share at least the outlook expressed in recent, model-based work on quasi-invariants (Binford & Levitt, 1993; Burns, Weiss, & Riseman, 1993), where strict invariance is relaxed; however, the functionals we compute are entirely different.

The invariance properties of the queries are related to the partial ordering and the manner in which they are selected during recursive partitioning. Roughly speaking, the complexity of the queries is proportional to the depth in the tree, that is, to the number of questions asked. For elementary queries at the bottom of the ordering, we would expect that for each class c , either $P(Q = 1|Y = c) \gg 0.5$ or $P(Q = 0|Y = c) \gg 0.5$; however this collection of elementary queries would have low discriminatory power. (These statements will be amplified later on.) Queries higher up in the ordering have much higher discriminatory power and maintain semi-invariance relative to subpopulations determined by the answers to queries preceding them in the ordering. Thus if \tilde{Q} is a query immediately preceding Q in the ordering, then $P(Q = 1|\tilde{Q} = 1, Y = c) \gg 0.5$ or $P(Q = 0|\tilde{Q} = 1, Y = c) \gg 0.5$ for each class c . This will be defined more precisely in section 5 and verified empirically.

Experiments on invariant recognition are scattered throughout the article. Some involve real data: handwritten digits. Most employ synthetic data, in which case the data model involves a prototype \mathbf{x}_c^* for each shape class $c \in \mathcal{C}$ (see Figure 1) together with a space Θ of image-to-image transformations. We assume that the class label of the prototype is preserved under all transformations in Θ , namely, $c = Y(\theta(\mathbf{x}_c^*))$ for all $\theta \in \Theta$, and that no two distinct prototypes can be transformed to the same image. We use “transformations” in a rather broad sense, referring to both affine maps, which alter the pose of the shapes, and to nonlinear maps, which deform the shapes. (We shall use *degradation* for noise, blur, etc.) Basically, Θ consists of *perturbations of the identity*. In particular, we are not considering the entire pose space but rather only perturbations of a reference pose, corresponding to the identity.

The probability measure P on \mathbf{X} is derived from a probability measure $\nu(d\theta)$ on the space of transformations as follows: for any $D \subset \mathbf{X}$,

$$P(D) = \sum_c P(D|Y = c)\pi(c) = \sum_c \nu\{\theta : \theta(\mathbf{x}_c^*) \in D\}\pi(c)$$

where π is a prior distribution on \mathcal{C} , which we will always take to be uniform. Thus, P is concentrated on the space of images $\{\theta(\mathbf{x}_c^*)\}_{\theta,c}$. Needless to say, the situation is more complex in many actual visual recognition problems, for example, in unrestricted 3D object recognition under standard projection models. Still, invariance is already challenging in the above context.

It is important to emphasize that this model is not used explicitly in the

classification algorithm. Knowledge of the prototypes is not assumed, nor is θ estimated as in template approaches. The purpose of the model is to generate samples for training and testing.

The images in Figure 2 were made by random sampling from a particular distribution ν on a space Θ containing both linear (scale, rotation, skew) and nonlinear transformations. Specifically, the log scale is drawn uniformly between $-1/6$ and $1/6$; the rotation angle is drawn uniformly from ± 10 degrees; and the log ratio of the axes in the skew is drawn uniformly from $-1/3$ to $+1/3$. The nonlinear part is a smooth, random deformation field constructed by creating independent, random horizontal and vertical displacements, each of which is generated by random trigonometric series with only low-frequency terms and gaussian coefficients. All images are 32×32 , but the actual size of the object in the image varies significantly, both from symbol to symbol and within symbol classes due to random scaling.

3 Shape Queries

We first illustrate a shape query in the context of curves and tangents in an idealized, continuum setting. The example is purely motivational. In practice we are not dealing with one-dimensional curves in the continuum but rather with a finite pixel lattice, strokes of variable width, corrupted data, and so forth. The types of queries we use are described in sections 3.1 and 3.2.

Observe the three versions of the digit “3” in Figure 3 (left); they are obtained by spline interpolation of the center points of the segments shown in Figure 3 (middle) in such a way that the segments represent the direction of the tangent at those points. All three segment arrangements satisfy the geometric relations indicated in Figure 3 (right): there is a vertical tangent northeast of a horizontal tangent, which is south of another horizontal tangent, and so forth. The directional relations between the points are satisfied to within rather coarse tolerances. Not all curves of a “3” contain five points whose tangents satisfy all these relations. Put differently, some “3”s answer “no” to the query, “Is there a vertical tangent northeast of a . . . ?” However, rather substantial transformations of each of the versions below will answer “yes.” Moreover, among “3”s that answer “no,” it is possible to choose a small number of alternative arrangements in such a way that the entire space of “3”s is covered.

3.1 Tags. We employ primitive local features called tags, which provide a coarse description of the local topography of the intensity surface in the neighborhood of a pixel. Instead of trying to manually characterize local configurations of interest—for example, trying to define local operators to identify gradients in the various directions—we adopt an information-theoretic approach and “code” a microworld of subimages by a process very similar to tree-structured vector quantization. In this way we sidestep the

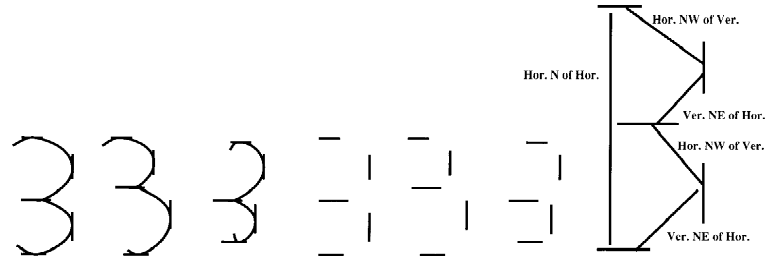


Figure 3: (Left) Three curves corresponding to the digit “3.” (Middle) Three tangent configurations determining these shapes via spline interpolation. (Right) Graphical description of relations between locations of derivatives consistent with all three configurations.

issues of boundary detection and gradients in the discrete world and allow for other forms of local topographies. This approach has been extended to gray level images in Jedynek and Fleuret (1996).

The basic idea is to reassign symbolic values to each pixel based on examining a few pixels in its immediate vicinity; the symbolic values are the tag types and represent labels for the local topography. The neighborhood we choose is the 4×4 subimage containing the pixel at the upper left corner. We cluster the subimages with binary splits corresponding to adaptively choosing the five most informative locations of the sixteen sites of the subimage.

Note that the size of the subimages used must depend on the resolution at which the shapes are imaged. The 4×4 subimages are appropriate for a certain range of resolutions—roughly 10×10 through 70×70 in our experience. The size must be adjusted for higher-resolution data, and the ultimate performance of the classifier will suffer if the resolution of the test data is not approximately the same as that of the training data. The best approach would be one that is multiresolution, something we have not done in this article (except for some preliminary experiments in section 11) but which is carried out in Jedynek and Fleuret (1996) in the context of gray-level images and 3D objects.

A large sample of 4×4 subimages is randomly extracted from the training data. The corresponding shape classes are irrelevant and are not retained. The reason is that the purpose of the sample is to provide a representative database of microimages and to discover the biases at that scale; the statistics of that world is largely independent of global image attributes, such as symbolic labels. This family of subimages is then recursively partitioned with binary splits. There are $4 \times 4 = 16$ possible questions: “Is site (i, j) black?” for $i, j = 1, 2, 3, 4$. The criterion for choosing a question at a node

t is dividing the subimages U_t at the node as equally as possible into two groups. This corresponds to reducing as much as possible the entropy of the empirical distribution on the 2^{16} possible binary configurations for the sample U_t . There is a tag type for each node of the resulting tree, except for the root. Thus, if three questions are asked, there are $2 + 4 + 8 = 14$ tags, and if five questions are asked, there are 62 tags. Depth 5 tags correspond to a more detailed description of the local topography than depth 3 tags, although eleven of the sixteen pixels still remain unexamined. Observe also that tags corresponding to internal nodes of the tree represent unions of those associated with deeper ones. At each pixel, we assign all the tags encountered by the corresponding 4×4 subimage as it proceeds down the tree. Unless otherwise stated, all experiments below use 62 tags.

At the first level, every site splits the population with nearly the same frequencies. However, at the second level, some sites are more informative than others, and by levels 4 and 5, there is usually one site that partitions the remaining subpopulation much better than all others. In this way, the world of microimages is efficiently coded. For efficiency, the population is restricted to subimages containing at least one black and one white site within the center four, which then obviously concentrates the processing in the neighborhood of boundaries. In the gray-level context it is also useful to consider more general tags, allowing, for example, for variations on the concept of local homogeneity.

The first three levels of the tree are shown in Figure 4, together with the most common configuration found at each of the eight level 3 nodes. Notice that the level 1 tag alone (i.e., the first bit in the code) determines the original image, so this “transform” is invertible and redundant. In Figure 5 we show all the two-bit tags and three-bit tags appearing in an image.

3.2 Tag Arrangements. The queries involve geometric arrangements of the tags. A query Q_A asks whether a specific geometric arrangement A of tags of certain types is present ($Q_A(\mathbf{x}) = 1$) or is not present ($Q_A(\mathbf{x}) = 0$) in the image. Figure 6 shows several \LaTeX symbols that contain a specific geometric arrangement of tags: tag 16 northeast of tag 53, which is northwest of tag 19. Notice that there are no fixed locations in this description, whereas the tags in any specific image do carry locations. “Present in the image” means there is at least one set of tags in \mathbf{x} of the prescribed types whose locations satisfy the indicated relationships. In Figure 6, notice, for example, how different instances of the digit “0” still contain the arrangement. Tag 16 is a depth 4 tag; the corresponding four questions in the subimage are indicated by the following mask:

$$\begin{pmatrix} n & n & n & 1 \\ 0 & n & n & n \\ n & 0 & 0 & n \\ n & n & n & n \end{pmatrix}$$

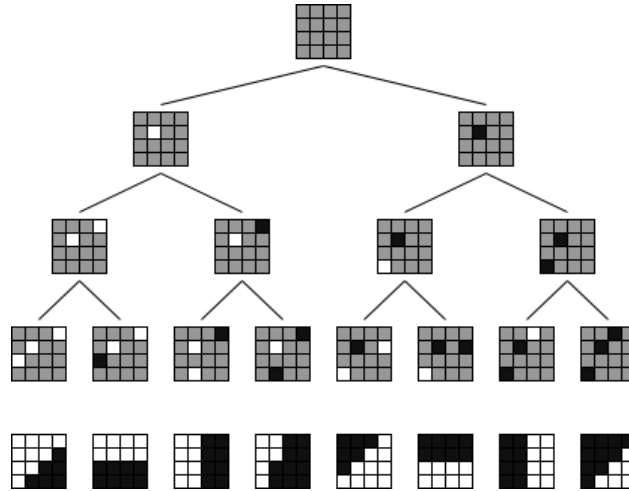


Figure 4: First three tag levels with most common configurations.

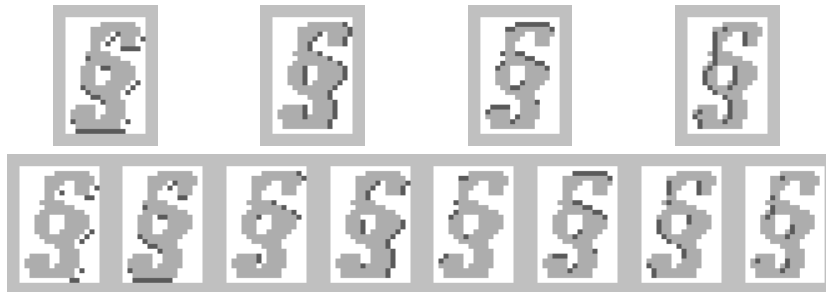


Figure 5: (Top) All instances of the four two-bit tags. (Bottom) All instances of the eight three-bit tags.

where 0 corresponds to background, 1 to object, and n to “not asked.” These neighborhoods are loosely described by “background to lower left, object to upper right.” Similar interpretations can be made for tags 53 and 19.

Restricted to the first ten symbol classes (the ten digits), the conditional distribution $P(Y = c | Q_A = 1)$ on classes given the existence of this arrangement in the image is given in Table 1. Already this simple query contains significant information about shape.

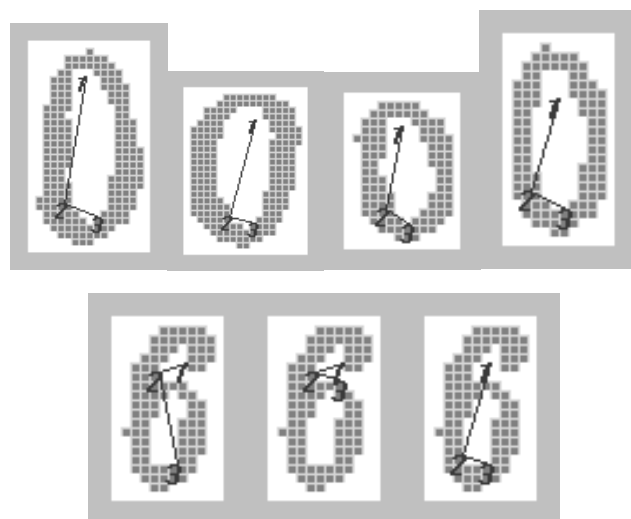


Figure 6: (Top) Instances of a geometric arrangement in several “0”s. (Bottom) Several instances of the geometric arrangement in one “6.”

Table 1: Conditional Distribution on Digit Classes Given the Arrangement of Figure 6.

0	1	2	3	4	5	6	7	8	9
.13	.003	.03	.08	.04	.07	.23	0	.26	.16

To complete the construction of the feature set, we need to define a set of allowable relationships among image locations. These are binary functions of pairs, triples, and so forth of planar points, which depend on only their relative coordinates. An arrangement \mathbf{A} is then a labeled (hyper)graph. Each vertex is labeled with a type of tag, and each edge (or superedge) is labeled with a type of relation. The graph in Figure 6, for example, has only binary relations. In fact, all the experiments on the \LaTeX symbols are restricted to this setting. The experiments on handwritten digits also use a ternary relationship of the metric type.

There are eight binary relations between any two locations u and v corresponding to the eight compass headings (north, northeast, east, etc.). For example, u is “north” of v if the angle of the vector $u - v$ is between $\pi/4$ and $3\pi/4$. More generally, the two points satisfy relation k ($k = 1, \dots, 8$) if the

angle of the vector $u - v$ is within $\pi/4$ of $k * \pi/4$. Let \mathcal{A} denote the set of all possible arrangements, and let $\mathbf{Q} = \{Q_{\mathbf{A}} : \mathbf{A} \in \mathcal{A}\}$, our feature set.

There are many other binary and ternary relations that have discriminating power. For example, there is an entire family of “metric” relationships that are, like the directional relationships above, completely scale and translation invariant. Given points u, v, w, z , one example of a ternary relation is $\|u - v\| < \|u - w\|$, which inquires whether u is closer to v than to w . With four points we might ask if $\|u - v\| < \|w - z\|$.

4 The Posterior Distribution and Tree-Based Approximations

For simplicity, and in order to facilitate comparisons with other methods, we restrict ourselves to queries $Q_{\mathbf{A}}$ of bounded complexity. For example, consider arrangements \mathbf{A} with at most twenty tags and twenty relations; this limit is never exceeded in any of the experiments. Enumerating these arrangements in some fashion, let $\mathbf{Q} = (Q_1, \dots, Q_M)$ be the corresponding feature vector assuming values in $\{0, 1\}^M$. Each image \mathbf{x} then generates a bit string of length M , which contains all the information available for estimating $Y(\mathbf{x})$. Of course, M is enormous. Nonetheless, it is not evident how we might determine a priori which features are informative and thereby reduce M to manageable size.

Evidently these bit strings partition \mathbf{X} . Two images that generate the same bit string or “atom” need not be identical. Indeed, due to the invariance properties of the queries, the two corresponding symbols may vary considerably in scale, location, and skew and are not even affine equivalent in general. Nonetheless, two such images will have very similar shapes. As a result, it is reasonable to expect that $H(Y|\mathbf{Q})$ (the conditional entropy of Y given \mathbf{Q}) is very small, in which case we can in principle obtain high classification rates using \mathbf{Q} .

To simplify things further, at least conceptually, we will assume that $H(Y|\mathbf{Q}) = 0$; this is not an unreasonable assumption for large M . An equivalent assumption is that the shape class Y is determined by \mathbf{Q} and the error rate of the Bayes classifier

$$\hat{Y}_B = \arg \max_c P(Y = c|\mathbf{Q})$$

is zero. Needless to say, perfect classification cannot actually be realized. Due to the size of M , the full posterior cannot be computed, and the classifier \hat{Y}_B is only hypothetical.

Suppose we examine some of the features by constructing a single binary tree T based on entropy-driven recursive partitioning and randomization and that T is uniformly of depth D so that D of the M features are examined for each image \mathbf{x} . (The exact procedure is described in the following section; the details are not important for the moment.) Suffice it to say that a feature Q_m is assigned to each interior node of T and the set of features $Q_{\pi_1}, \dots, Q_{\pi_D}$

along each branch from root to leaf is chosen sequentially and based on the current information content given the observed values of the previously chosen features. The classifier based on T is then

$$\begin{aligned}\hat{Y}_T &= \arg \max_c P(Y = c|T) \\ &= \arg \max_c P(Y = c|Q_{\pi_1}, \dots, Q_{\pi_D})\end{aligned}$$

since $D \ll M$, \hat{Y}_T is not the Bayes classifier. However, even for values of D on the order of hundreds or thousands, we can expect that

$$P(Y = c|T) \approx P(Y = c|Q).$$

We shall refer to the difference between these distributions (in some appropriate norm) as the approximation error (AE). This is one of the sources of error in replacing Q by a subset of features. Of course, we cannot actually compute a tree of such depth since at least several hundred features are needed to achieve good classification; we shall return to this point shortly.

Regardless of the depth D , in reality we do not actually know the posterior distribution $P(Y = c|T)$. Rather, it must be estimated from a training set $\mathcal{L} = \{(\mathbf{x}_1, Y(\mathbf{x}_1)), \dots, (\mathbf{x}_m, Y(\mathbf{x}_m))\}$, where $\mathbf{x}_1, \dots, \mathbf{x}_m$ is a random sample from P . (The training set is also used to estimate the entropy values during recursive partitioning.) Let $\hat{P}_{\mathcal{L}}(Y = c|T)$ denote the estimated distribution, obtained by simply counting the number of training images of each class c that land at each terminal node of T . If \mathcal{L} is sufficiently large, then

$$\hat{P}_{\mathcal{L}}(Y = c|T) \approx P(Y = c|T).$$

We call the difference estimation error (EE), which of course vanishes only as $|\mathcal{L}| \rightarrow \infty$.

The purpose of multiple trees (see section 6) is to solve the approximation error problem and the estimation error problem at the same time. Even if we could compute and store a very deep tree, there would still be too many probabilities (specifically $K2^D$) to estimate with a practical training set \mathcal{L} . Our approach is to build multiple trees T_1, \dots, T_N of modest depth. In this way tree construction is practical and

$$\hat{P}_{\mathcal{L}}(Y = c|T_n) \approx P(Y = c|T_n), \quad n = 1, \dots, N.$$

Moreover, the total number of features examined is sufficiently large to control the approximation error. The classifier we propose is

$$\hat{Y}_S = \arg \max_c \frac{1}{N} \sum_{n=1}^N \hat{P}_{\mathcal{L}}(Y = c|T_n).$$

An explanation for this particular way of aggregating the information from multiple trees is provided in section 6.1. In principle, a better way to combine the trees would be to classify based on the mode of $P(Y = c|T_1, \dots, T_N)$.

However, this is impractical for reasonably sized training sets for the same reasons that a single deep tree is impractical (see section 6.4 for some numerical experiments). The trade-off between AE and EE is related to the trade-off between bias and variance, which is discussed in section 6.2, and the relative error rates among all these classifiers is analyzed in more detail in section 6.4 in the context of parameter estimation.

5 Tree-Structured Shape Quantization

Standard decision tree construction (Breiman et al., 1984; Quinlan, 1986) is based on a scalar-valued feature or attribute vector $\mathbf{z} = (z_1, \dots, z_k)$ where k is generally about 10 – 100. Of course, in pattern recognition, the raw data are images, and finding the right attributes is widely regarded as the main issue. Standard splitting rules are based on functions of this vector, usually involving a single component z_j (e.g., applying a threshold) but occasionally involving multivariate functions or “transgenerated features” (Friedman, 1973; Gelfand & Delp, 1991; Guo & Gelfand, 1992; Sethi, 1991). In our case, the queries $\{Q_A\}$ are the candidates for splitting rules. We now describe the manner in which the queries are used to construct a tree.

5.1 Exploring Shape Space. Since the set of queries \mathbf{Q} is indexed by graphs, there is a natural partial ordering under which a graph precedes any of its extensions. The partial ordering corresponds to a hierarchy of structure. Small arrangements with few tags produce coarse splits of shape space. As the arrangements increase in size (say, the number of tags plus relations), they contain more and more information about the images that contain them. However, fewer and fewer images contain such an instance—that is, $P(Q = 1) \approx 0$ for a query Q based on a complex arrangement.

One straightforward way to exploit this hierarchy is to build a decision tree using the collection \mathbf{Q} as candidates for splitting rules, with the complexity of the queries increasing with tree depth (distance from the root). In order to begin to make this computationally feasible, we define a *minimal extension* of an arrangement \mathbf{A} to mean the addition of exactly one relation between existing tags, or the addition of exactly one tag and one relation binding the new tag to an existing one. By a *binary arrangement*, we mean one with two tags and one relation; the collection of associated queries is denoted $\mathbf{B} \subset \mathbf{Q}$.

Now build a tree as follows. At the root, search through \mathbf{B} and choose the query $Q \in \mathbf{B}$, which leads to the greatest reduction in the mean uncertainty about Y given Q . This is the standard criterion for recursive partitioning in machine learning and other fields. Denote the chosen query Q_{A_0} . Those data points for which $Q_{A_0} = 0$ are in the “no” child node, and we search again through \mathbf{B} . Those data points for which $Q_{A_0} = 1$ are in the “yes” child node and have one or more instances of \mathbf{A}_0 , the “pending arrangement.” Now search among minimal extensions of \mathbf{A}_0 and choose the one that leads

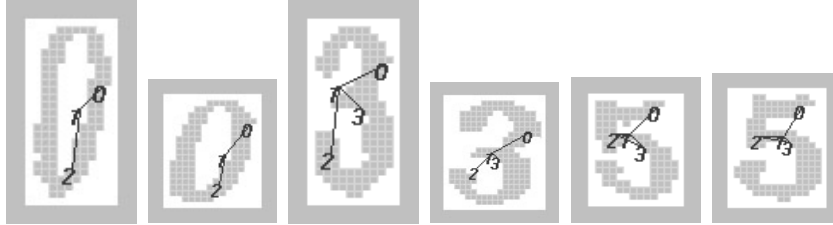


Figure 7: Examples of node splitting. All six images lie in the same node and have a pending arrangement with three vertices. The “0”s are separated from the “3”s and “5”s by asking for the presence of a new tag, and then the “3”s and “5”s are separated by asking a question about the relative angle between two existing vertices. The particular tags associated with these vertices are not indicated.

to the greatest reduction in uncertainty about Y given the existence of A_0 . The digits in Figure 6 were taken from a depth 2 (“yes”/“yes”) node of such a tree.

We measure uncertainty by Shannon entropy. The expected uncertainty in Y given a random variable Z is

$$H(Y|Z) = - \sum_z P(Z = z) \sum_c P(Y = c|Z = z) \log_2 P(Y = c|Z = z).$$

Define $H(Y|Z, B)$ for an event $B \subset \mathbf{X}$ in the same way, except that P is replaced by the conditional probability measure $P(\cdot|B)$.

Given we are at a node t of depth $k > 0$ in the tree, let the “history” be $B_t = \{Q_{A_0} = q_0, \dots, Q_{A_{k-1}} = q_{k-1}\}$, meaning that Q_{A_1} is the second query chosen given that $q_0 \in \{0, 1\}$ is the answer to the first; Q_{A_2} is the third query chosen given the answers to the first two are q_0 and q_1 ; and so forth. The pending arrangement, say A_j , is the deepest arrangement along the path from root to t for which $q_j = 1$, so that $q_i = 0, i = j + 1, \dots, k - 1$. Then Q_{A_k} minimizes $H(Y|Q_A, B_t)$ among minimal extensions of A_j . An example of node splitting is shown in Figure 7. Continue in this fashion until a stopping criterion is satisfied, for example, the number of data points at every terminal node falls below a threshold. Each tree may then be regarded as a discrete random variable T on \mathbf{X} ; each terminal node corresponds to a different value of T .

In practice, we cannot compute these expected entropies; we can only estimate them from a training set \mathcal{L} . Then P is replaced by the empirical distribution $\hat{P}_{\mathcal{L}}$ on $\{\mathbf{x}_1, \dots, \mathbf{x}_m\}$ in computing the entropy values.

5.2 Randomization. Despite the growth restrictions, the procedure above is still not practical; the number of binary arrangements is very large, and

there are too many minimal extensions of more complex arrangements. In addition, if more than one tree is made, even with a fresh sample of data points per tree, there might be very little difference among the trees. The solution is simple: instead of searching among all the admissible queries at each node, we restrict the search to a small random subset.

5.3 A Structural Description. Notice that only *connected* arrangements can be selected, meaning every two tags are *neighbors* (participate in a relation) or are connected by a sequence of neighboring tags. As a result, training is more complex than standard recursive partitioning. At each node, a list must be assigned to each data point consisting of all instances of the pending arrangement, including the coordinates of each participating tag. If a data point passes to the “yes” child, then only those instances that can be incremented are maintained and updated; the rest are deleted. The more data points there are, the more bookkeeping.

A far simpler possibility is sampling exclusively from \mathbf{B} , the binary arrangements (i.e., two vertices and one relation) listed in some order. In fact, we can imagine evaluating all the queries in \mathbf{B} for each data point. This vector could then be used with a variety of standard classifiers, including decision trees built in the standard fashion. In the latter case, the pending arrangements are unions of binary graphs, each one disconnected from all the others. This approach is much simpler and faster to implement and preserves the semi-invariance. However, the price is dear: losing the common, global characterization of shape in terms of a large, connected graph. Here we are referring to the pending arrangements at the terminal nodes (except at the end of the all “no” branch); by definition, this graph is found in all the shapes at the node. This is what we mean by a *structural description*. The difference between one connected graph and a union of binary graphs can be illustrated as follows. Relative to the entire population \mathbf{X} , a random selection in \mathbf{B} is quite likely to carry some information about Y , measured, say, by the mutual information $I(Y, Q) = H(Y) - H(Y|Q)$. On the other hand, a random choice among all queries with, say, five tags will most likely have no information because nearly all data points \mathbf{x} will answer “no.” In other words, it makes sense at least to start with binary arrangements.

Assume, however, that we are restricted to a subset $\{Q_{\mathbf{A}} = 1\} \subset \mathbf{X}$ determined by an arrangement \mathbf{A} of moderate complexity. (In general, the subsets at the nodes are determined by the “no” answers as well as the “yes” answers, but the situation is virtually the same.) On this small subset, a randomly sampled binary arrangement will be less likely to yield a significant drop in uncertainty than a randomly sampled query among minimal extensions of \mathbf{A} . These observations have been verified experimentally, and we omit the details.

This distinction becomes more pronounced if the images are noisy (see the top panel of Figure 8) or contain structured backgrounds (see the bottom panel of Figure 11) because there will be many false positives for ar-

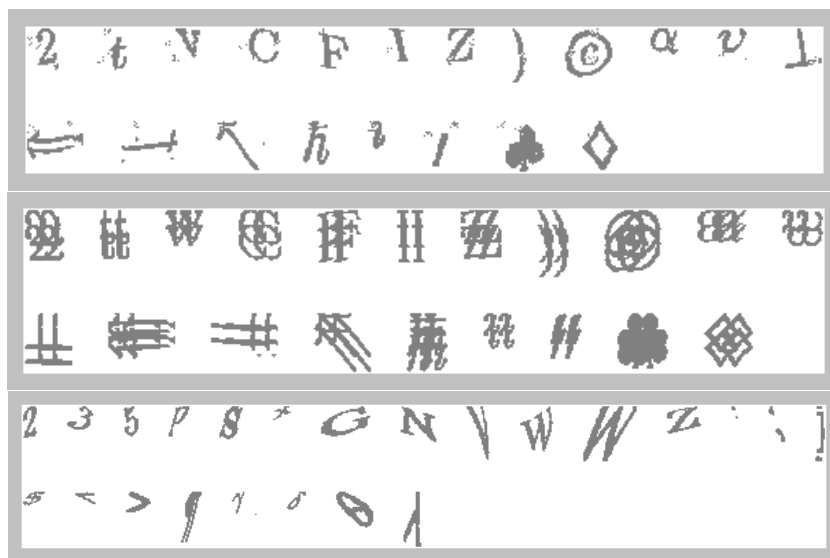


Figure 8: Samples from data sets. (Top) Spot noise. (Middle) Duplication. (Bottom) Severe perturbations.

rangements with only two tags. However, the chance of finding complex arrangements utilizing noise tags or background tags is much smaller. Put differently, a structural description is more robust than a list of attributes. The situation is the same for more complex shapes; see, for example, the middle panel of Figure 8, where the shapes were created by duplicating each symbol four times with some shifts. Again, a random choice among minimal extensions carries much more information than a random choice in \mathbf{B} .

5.4 Semi-Invariance. Another benefit of the structural description is what we refer to as semi-invariance. Given a node t , let B_t be the history and \mathbf{A}_j the pending arrangement. For any minimal extension \mathbf{A} of \mathbf{A}_j , and for any shape class c , we want

$$\max(P(Q_{\mathbf{A}} = 0 | Y = c, B_t), P(Q_{\mathbf{A}} = 1 | Y = c, B_t)) \gg .5.$$

In other words, most of the images in B_t of the same class should answer the same way to query $Q_{\mathbf{A}}$. In terms of entropy, semi-invariance is equivalent to relatively small values of $H(Q_{\mathbf{A}} | Y = c, B_t)$ for all c . Averaging over classes, this in turn is equivalent to small values of $H(Q_{\mathbf{A}} | Y, B_t)$ at each node t .

In order to verify this property we created ten trees of depth 5 using the data set described in section 2 with thirty-two samples per symbol class.

At each nonterminal node t of each tree, the average value of $H(Q_A|Y, B_t)$ was calculated over twenty randomly sampled minimal extensions. Over all nodes, the mean entropy was $m = .33$; this is the entropy of the distribution $(.06, .94)$. The standard deviation over all nodes and queries was $\sigma = .08$. Moreover, there was a clear decrease in average entropy (i.e., increase in the degree of invariance) as the depth of the node increases.

We also estimated the entropy for more severe deformations. On a more variable data set with approximately double the range of rotations, log scale, and log skew (relative to the values in section 2), and the same nonlinear deformations, the corresponding numbers were $m = .38$, $\sigma = .09$. Finally for rotations sampled from $(-30, 30)$ degrees, log scale from $(-.5, .5)$, log skew from $(-1, 1)$, and doubling the variance of the random nonlinear deformation (see the bottom panel of Figure 8), the corresponding mean entropy was $m = .44$ ($\sigma = .11$), corresponding to a $(.1, .9)$ split. In other words, on average, 90 percent of the images in the same shape class still answer the same way to a new query.

Notice that invariance property is independent of the discriminating power of the query, that is, the extent to which the distribution $P(Y = c|B_t, Q_A)$ is more peaked than the distribution $P(Y = c|B_t)$. Due to the symmetry of mutual information,

$$H(Y|B_t) - H(Y|Q_A, B_t) = H(Q_A|B_t) - H(Q_A|Y, B_t).$$

This means that if we seek a question that maximizes the reduction in the conditional entropy of Y and assume the second term on the right is small due to semi-invariance, then we need only find a query that maximizes $H(Q_A|B_t)$. This, however, does not involve the class variable and hence points to the possibility of unsupervised learning, which is discussed in the following section.

5.5 Unsupervised Learning. We outline two ways to construct trees in an unsupervised mode, that is, without using the class labels $Y(x_j)$ of the samples x_j in \mathcal{L} . Clearly each query Q_m decreases uncertainty about Q , and hence about Y . Indeed, $H(Y|Q_m) \leq H(Q|Q_m)$ since we are assuming Y is determined by Q . More generally, if T is a tree based on some of the components of Q and if $H(Q|T) \ll H(Q)$, then T should contain considerable information about the shape class. Recall that in the supervised mode, the query Q_m chosen at node t minimizes $H(Y|B_t, Q_m)$ (among a random sample of admissible queries), where B_t is the event in \mathbf{X} corresponding to the answers to the previous queries. Notice that typically this is not equivalent to simply maximizing the information content of Q_m because $H(Y|B_t, Q_m) = H(Y, Q_m|B_t) - H(Q_m|B_t)$, and both terms depend on m . However, in the light of the discussion in the preceding section about semi-invariance, the first term can be ignored, and we can focus on maximizing the second term.

Another way to motivate this criterion is to replace Y by \mathbf{Q} , in which case

$$\begin{aligned} H(\mathbf{Q}|B_t, Q_m) &= H(\mathbf{Q}, Q_m|B_t) - H(Q_m|B_t) \\ &= H(\mathbf{Q}|B_t) - H(Q_m|B_t). \end{aligned}$$

Since the first term is independent of m , the query of choice will again be the one maximizing $H(Q_m|B_t)$. Recall that the entropy values are estimated from training data and that Q_m is binary. It follows that growing a tree aimed at reducing uncertainty about \mathbf{Q} is equivalent to finding at each node that query which best splits the data at the node into two equal parts. This results from the fact that maximizing $H(p) = p \log_2(p) + (1-p) \log_2(1-p)$ reduces to minimizing $|p - .5|$.

In this way we generate *shape quantiles* or clusters ignoring the class labels. Still, the tree variable T is highly correlated with the class variable Y . This would be the case even if the tree were grown from samples representing only some of the shape classes. In other words, these clustering trees produce a *generic quantization* of shape space. In fact, the same trees can be used to classify new shapes (see section 9).

We have experimented with such trees, using the splitting criterion described above as well as another unsupervised one based on the “question metric,”

$$d_{\mathbf{Q}}(\mathbf{x}, \mathbf{x}') = \frac{1}{M} \sum_{m=1}^M \delta(Q_m(\mathbf{x}) \neq Q_m(\mathbf{x}')), \quad \mathbf{x}, \mathbf{x}' \in \mathbf{X}$$

where $\delta(\dots) = 1$ if the statement is true and $\delta(\dots) = 0$ otherwise. Since \mathbf{Q} leads to Y , it makes sense to divide the data so that each child is as homogeneous as possible with respect to $d_{\mathbf{Q}}$; we omit the details. Both clustering methods lead to classification rates that are inferior to those obtained with splits determined by separating classes but still surprisingly high; one such experiment is reported in section 6.1.

6 Multiple Trees

We have seen that small, random subsets of the admissible queries at any node invariably contain at least one query that is informative about the shape class. What happens if many such trees are constructed using the same training set \mathcal{L} ? Because the family \mathbf{Q} of queries is so large and because different queries—tag arrangements—address different aspects of shape, separate trees should provide separate structural descriptions, characterizing the shapes from different “points of view.” This is illustrated in Figure 9, where the same image is shown with an instance of the pending graph at the terminal node in five different trees. Hence, aggregating the information provided by a family of trees (see section 6.1) should yield more accurate and more robust classification. This will be demonstrated in experiments throughout the remainder of the article.

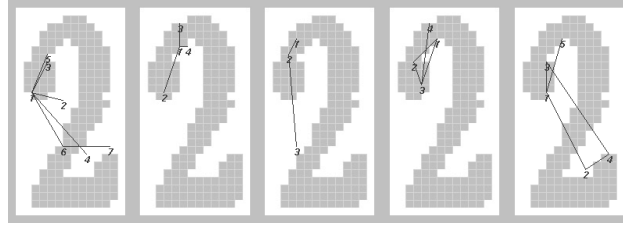


Figure 9: Graphs found in an image at terminal nodes of five different trees.

Generating multiple trees by randomization was proposed in Geman, Amit, & Wilder (1996). Previously, other authors had advanced other methods for generating multiple trees. One of the earliest was weighted voting trees (Casey & Jih, 1983); Shlien (1990) uses different splitting criteria; Breiman (1994) uses bootstrap replicates of \mathcal{L} ; and Dietterich and Bakiri (1995) introduce the novel idea of replacing the multiclass learning problem by a family of two-class problems, dedicating a tree to each of these. Most of these articles deal with fixed-size feature vectors and coordinate-based questions. All authors report gains in accuracy and stability.

6.1 Aggregation. Suppose we are given a family of trees T_1, \dots, T_N . The best classifier based on these is

$$\hat{Y}_A = \arg \max_c P(Y = c | T_1, \dots, T_N),$$

but this is not feasible (see section 6.4). Another option would be to regard the trees as high-dimensional inputs to standard classifiers. We tried that with classification trees, linear and nonlinear discriminant analysis, K-means clustering, and nearest neighbors, all without improvement over simple averaging for the amount of training data we used.

By averaging, we mean the following. Let $\mu_{n,\tau}(c)$ denote the posterior distribution $P(Y = c | T_n = \tau)$, $n = 1, \dots, N$, $c = 1, \dots, K$, where τ denotes a terminal node. We write μ_{T_n} for the random variable μ_{n,T_n} . These probabilities are the parameters of the system, and the problem of estimating them will be discussed in section 6.4. Define

$$\bar{\mu}(\mathbf{x}) = \frac{1}{N} \sum_{n=1}^N \mu_{T_n}(\mathbf{x}),$$

the arithmetic average of the distributions at the leaves reached by \mathbf{x} . The mode of $\bar{\mu}(\mathbf{x})$ is the class assigned to the data point \mathbf{x} , that is,

$$\hat{Y}_S = \arg \max_c \bar{\mu}_c.$$

Using a training database of thirty-two samples per symbol from the distribution described in section 2, we grew $N = 100$ trees of average depth $d = 10$, and tested the performance on a test set of five samples per symbol. The classification rate was 96 percent. This experiment was repeated several times with very similar results. On the other hand, growing one hundred unsupervised trees of average depth 11 and using the labeled data only to estimate the terminal distributions, we achieved a classification rate of 94.5 percent.

6.2 Dependence on the Training Set. The performance of classifiers constructed from training samples can be adversely affected by overdependence on the particular sample. One way to measure this is to consider the population of all training sets \mathcal{L} of a particular size and to compute, for each data point \mathbf{x} , the average $E_{\mathcal{L}} e_{\mathcal{L}}(\mathbf{x})$, where $e_{\mathcal{L}}$ denotes the error at \mathbf{x} for the classifier made with \mathcal{L} . (These averages may then be further averaged over \mathbf{X} .) The average error decomposes into two terms, one corresponding to bias and the other to variance (Geman, Bienenstock, & Doursat, 1992). Roughly speaking, the bias term captures the systematic errors of the classifier design, and the variance term measures the error component due to random fluctuations from \mathcal{L} to \mathcal{L} . Generally parsimonious designs (e.g., those based on relatively few unknown parameters) yield low variance but highly biased decision boundaries, whereas complex nonparametric classifiers (e.g., neural networks with many parameters) suffer from high variance, at least without enormous training sets. Good generalization requires striking a balance. (See Geman et al., 1992, for a comprehensive treatment of the bias/variance dilemma; see also the discussions in Breiman, 1994; Kong & Dietterich, 1995; and Raudys & Jain, 1991.)

One simple experiment was carried out to measure the dependence of our classifier \hat{Y}_S on the training sample; we did not systematically explore the decomposition mentioned above. We made ten sets of twenty trees from ten different training sets, each consisting of thirty-two samples per symbol. The average classification rate was 85.3 percent; the standard deviation was 0.8 percent. Table 2 shows the number of images in the test set correctly labeled by j of the classifiers, $j = 0, 1, \dots, 10$. For example, we see that 88 percent of the test points are correctly labeled at least six out of ten times. Taking the plurality of the ten classifiers improves the classification rate to 95.5 percent so there is some pointwise variability among the classifiers. However, the decision boundaries and overall performance are fairly stable with respect to \mathcal{L} .

We attribute the relatively small variance component to the aggregation of many weakly dependent trees, which in turn results from randomization. The bias issue is more complex, and we have definitely noticed certain types of structural errors in our experiments with handwritten digits from the NIST database; for example, certain styles of writing are systematically misclassified despite the randomization effects.

Table 2: Number of Points as a Function of the Number of Correct Classifiers.

Number of correct classifiers	0	1	2	3	4	5	6	7	8	9	10
Number of points	9	11	20	29	58	42	59	88	149	237	763

6.3 Relative Error Rates. Due to estimation error, we favor many trees of modest depth over a few deep ones, even at the expense of theoretically higher error rates where perfect estimation is possible. In this section, we analyze those error rates for some of the alternative classifiers discussed above in the asymptotic case of infinite data and assuming the total number of features examined is held fixed, presumably large enough to guarantee low approximation error. The implications for finite data are outlined in section 6.4.

Instead of making N trees T_1, \dots, T_N of depth D , suppose we made just one tree T^* of depth ND ; in both cases we are asking ND questions. Of course this is not practical for the values of D and N mentioned above (e.g., $D = 10$, $N = 20$), but it is still illuminating to compare the hypothetical performance of the two methods. Suppose further that the criterion for selecting T^* is to minimize the error rate over all trees of depth ND :

$$T^* = \arg \max_T E[\max_c P(Y = c|T)],$$

where the maximum is over all trees of depth ND . The error rate of the corresponding classifier $\hat{Y}^* = \arg \max_c P(Y = c|T^*)$ is then $e(\hat{Y}^*) = 1 - E[\max_c P(Y = c|T^*)]$. Notice that finding T^* would require the solution of a global optimization problem that is generally intractable, accounting for the nearly universal adoption of greedy tree-growing algorithms based on entropy reduction, such as the one we are using. Notice also that minimizing the entropy $H(Y|T)$ or the error rate $P(Y \neq \hat{Y}(T))$ amounts to basically the same thing.

Let $e(\hat{Y}_A)$ and $e(\hat{Y}_S)$ be the error rates of \hat{Y}_A and \hat{Y}_S (defined in 6.1), respectively. Then it is easy to show that

$$e(\hat{Y}^*) \leq e(\hat{Y}_A) \leq e(\hat{Y}_S).$$

The first inequality results from the observation that the N trees of depth D could be combined into one tree of depth ND simply by grafting T_2 onto each terminal node of T_1 , then grafting T_3 onto each terminal node of the new tree, and so forth. The error rate of the tree so constructed is just $e(\hat{Y}_A)$. However, the error rate of T^* is minimal among all trees of depth ND , and hence is lower than $e(\hat{Y}_A)$. Since \hat{Y}_S is a function of T_1, \dots, T_N , the second inequality follows from a standard argument:

$$\begin{aligned}
P(Y \neq \hat{Y}_S) &= E[P(Y \neq \hat{Y}_S | T_1, \dots, T_N)] \\
&\geq E[P(Y \neq \arg \max_c P(Y = c | T_1, \dots, T_N)) | T_1, \dots, T_N] \\
&= P(Y \neq \hat{Y}_A).
\end{aligned}$$

6.4 Parameter Estimation. In terms of tree depth, the limiting factor is parameter estimation, not computation or storage. The probabilities $P(Y = c | T^*)$, $P(Y = c | T_1, \dots, T_N)$, and $P(Y = c | T_n)$ are unknown and must be estimated from training data. In each of the cases \hat{Y}^* and \hat{Y}_A , there are $K \times 2^{ND}$ parameters to estimate (recall K is the number of shape classes), whereas for \hat{Y}_S there are $K \times N \times 2^D$ parameters. Moreover, the number of data points in \mathcal{L} available per parameter is $\|\mathcal{L}\|/(K2^{ND})$ in the first two cases and $\|\mathcal{L}\|/(K2^D)$ with aggregation.

For example, consider the family of $N = 100$ trees described in section 6.1, which were used to classify the $K = 293$ L^AT_EX symbols. Since the average depth is $D = 8$, then there are approximately $100 \times 2^8 \times 293 \sim 7.5 \times 10^6$ parameters, although most of these are nearly zero. *Indeed, in all experiments reported below, only the largest five elements of $\mu_{n,\tau}$ are estimated; the rest are set to zero.* It should be emphasized, however, that the parameter estimates can be refined indefinitely using additional samples from \mathbf{X} , a form of incremental learning (see section 9).

For $\hat{Y}_A = \arg \max_c P(Y = c | T_1, \dots, T_N)$ the estimation problem is overwhelming, at least without assuming conditional independence or some other model for dependence. This was illustrated when we tried to compare the magnitudes of $e(\hat{Y}_A)$ with $e(\hat{Y}_S)$ in a simple case. We created $N = 4$ trees of depth $D = 5$ to classify just the first $K = 10$ symbols, which are the ten digits. The trees were constructed using a training set \mathcal{L} with 1000 samples per symbol. Using \hat{Y}_S , the error rate on \mathcal{L} was just under 6 percent; on a test set \mathcal{V} of 100 samples per symbol, the error rate was 7 percent.

Unfortunately \mathcal{L} was not large enough to estimate the full posterior given the four trees. Consequently, we tried using 1000, 2000, 4000, 10,000, and 20,000 samples per symbol for estimation. With two trees, the error rate was consistent from \mathcal{L} to \mathcal{V} , even with 2000 samples per symbol, and it was slightly lower than $e(\hat{Y}_S)$. With three trees, there was a significant gap between the (estimated) $e(\hat{Y}_A)$ on \mathcal{L} and \mathcal{V} , even with 20,000 samples per symbol; the estimated value of $e(\hat{Y}_A)$ on \mathcal{V} was 6 percent compared with 8 percent for $e(\hat{Y}_S)$. With four trees and using 20,000 samples per symbol, the estimate of $e(\hat{Y}_A)$ on \mathcal{V} was about 6 percent, and about 1 percent on \mathcal{L} . It was only 1 percent better than $e(\hat{Y}_S)$, which was 7 percent and required only 1000 samples per symbol.

We did not go beyond 20,000 samples per symbol. Ultimately \hat{Y}_A will do better, but the amount of data needed to demonstrate this is prohibitive, even for four trees. Evidently the same problems would be encountered in trying to estimate the error rate for a very deep tree.

7 Performance Bounds

We divide this into two cases: individual trees and multiple trees. Most of the analysis for individual trees concerns a rather ideal case (twenty questions) in which the shape classes are atomic; there is then a natural metric on shape classes, and one can obtain bounds on the expected uncertainty after a given number of queries in terms of this metric and an initial distribution over classes. The key issue for multiple trees is weak dependence, and the analysis there is focused on the dependence structure among the trees.

7.1 Individual Trees: Twenty Questions. Suppose first that each shape class or hypothesis c is atomic, that is, it consists of a single atom of \mathcal{Q} (as defined in section 4). In other words each “hypothesis” c has a unique code word, which we denote by $\mathbf{Q}(c) = (Q_1(c), \dots, Q_M(c))$, so that \mathbf{Q} is determined by Y . This setting corresponds exactly to a mathematical version of the twenty questions game. There is also an initial distribution $\nu(c) = P(Y = c)$. For each $c = 1, \dots, K$, the binary sequence $(Q_m(1), \dots, Q_m(K))$ determines a subset of hypotheses—those that answer yes to query Q_m . Since the code words are distinct, asking enough questions will eventually determine Y . The mathematical problem is to find the ordering of the queries that minimizes the mean number of queries needed to determine Y or the mean uncertainty about Y after a fixed number of queries. The best-known example is when there is a query for every subset of $\{1, \dots, K\}$, so that $M = 2^K$. The optimal strategy is given by the Huffman code, in which case the mean number of queries required to determine Y lies in the interval $[H(Y), H(Y) + 1)$ (see Cover & Thomas, 1991).

Suppose π_1, \dots, π_k represent the indices of the first k queries. The mean residual uncertainty about Y after k queries is then

$$\begin{aligned} H(Y|Q_{\pi_1}, \dots, Q_{\pi_k}) &= H(Y, Q_{\pi_1}, \dots, Q_{\pi_k}) - H(Q_{\pi_1}, \dots, Q_{\pi_k}) \\ &= H(Y) - H(Q_{\pi_1}, \dots, Q_{\pi_k}) \\ &= H(Y) - (H(Q_{\pi_1}) + H(Q_{\pi_2}|Q_{\pi_1}) \\ &\quad + \dots + H(Q_{\pi_k}|Q_{\pi_1}, \dots, Q_{\pi_{k-1}})). \end{aligned}$$

Consequently, if at each stage there is a query that divides the active hypotheses into two groups such that the mass of the smaller group is at least β ($0 < \beta \leq .5$), then $H(Y|Q_{\pi_1}, \dots, Q_{\pi_k}) \leq H(Y) - kH(\beta)$. The mean decision time is roughly $H(Y)/H(\beta)$. In all unsupervised trees we produced, we found $H(Q_{\pi_k}|Q_{\pi_1}, \dots, Q_{\pi_{k-1}})$ to be greater than .99 (corresponding to $\beta \approx .5$) at 95 percent of the nodes.

If assumptions are made about the degree of separation among the code words, one can obtain bounds on mean decision times and the expected uncertainty after a fixed number of queries, in terms of the prior distribution ν . For these types of calculations, it is easier to work with the Hellinger

measure of uncertainty than with Shannon entropy. Given a probability vector $\mathbf{p} = (p_1, \dots, p_J)$, define

$$G(\mathbf{p}) = \sum_{j \neq i} \sqrt{p_j} \sqrt{p_i},$$

and define $G(Y)$, $G(Y|B_t)$, and $G(Y|B_t, Q_m)$ the same way as with the entropy function H . (G and H have similar properties; for example, G is minimized on a point mass, maximized on the uniform distribution, and it follows from Jensen's inequality that $H(\mathbf{p}) \leq \log_2[G(\mathbf{p}) + 1]$.) The initial amount of uncertainty is

$$G(Y) = \sum_{c \neq c'} v^{1/2}(c) v^{1/2}(c').$$

For any subset $\{m_1, \dots, m_k\} \subset \{1, \dots, M\}$, using Bayes rule and the fact that $P(Q|Y)$ is either 0 or 1, we obtain

$$G(Y|Q_{m_1}, \dots, Q_{m_k}) = \sum_{c \neq c'} \prod_{i=1}^k \delta(Q_{m_i}(c) = Q_{m_i}(c')) v^{1/2}(c) v^{1/2}(c').$$

Now suppose we average $G(Y|Q_{m_1}, \dots, Q_{m_k})$ over all subsets $\{m_1, \dots, m_k\}$ (allowing repetition). The average is

$$\begin{aligned} M^{-k} \sum_{(m_1, \dots, m_k)} G(Y|Q_{m_1}, \dots, Q_{m_k}) &= \sum_{c \neq c'} M^{-k} \sum_{(m_1, \dots, m_k)} \prod_{i=1}^k \\ &\quad \times \delta(Q_{m_i}(c) = Q_{m_i}(c')) v^{1/2}(c) v^{1/2}(c') \\ &= \sum_{c \neq c'} (1 - d_Q(c, c'))^k v^{1/2}(c) v^{1/2}(c'). \end{aligned}$$

Consequently, any better-than-average subset of queries satisfies

$$G(Y|Q_{m_1}, \dots, Q_{m_k}) \leq \sum_{c \neq c'} (1 - d_Q(c, c'))^k v^{1/2}(c) v^{1/2}(c').$$

If $\gamma = \min_{c, c'} d_Q(c, c')$, then the residual uncertainty is at most $(1 - \gamma)^k G(Y)$. In order to disambiguate K hypotheses under a uniform starting distribution (in which case $G(Y) = K - 1$) we would need approximately

$$k \approx -\frac{\log K}{\log(1 - \gamma)}$$

queries, or $k \approx \log K / \gamma$ for small γ . (This is clear without the general inequality above, since we eliminate a fraction γ of the remaining hypotheses with each new query.) This value of k is too large to be practical for realistic values of γ (due to storage, etc.) but does express the divide-and-conquer nature

of recursive partitioning in the logarithmic dependence on the number of hypotheses.

Needless to say, the compound case is the only realistic one, where the number of atoms in a shape class is a measure of its complexity. (For example, we would expect many more atoms per handwritten digit class than per printed font class.) In the compound case, one can obtain results similar to those mentioned above by considering the degree of homogeneity within classes as well as the degree of separation between classes. For example, the index γ must be replaced by one based on both the maximum distance D_{\max} between code words of the same class and the minimum distance D_{\min} between code words from different classes. Again, the bounds obtained call for trees that are too deep actually to be made, and much deeper than those that are empirically demonstrated to obtain good discrimination. We achieve this in practice due to semi-invariance, guaranteeing that D_{\max} is small, and the extraordinary richness of the world of spatial relationships, guaranteeing that D_{\min} is large.

7.2 Multiple Trees: Weak Dependence. From a statistical perspective, randomization leads to weak conditional dependence among the trees. For example, given $Y = c$, the correlation between two trees T_1 and T_2 is small. In other words, given the class of an image, knowing the leaf of T_1 that is reached would not aid us in predicting the leaf reached in T_2 .

In this section, we analyze the dependence structure among the trees and obtain a crude lower bound on the performance of the classifier \hat{Y}_S for a fixed family of trees T_1, \dots, T_N constructed from a fixed training set \mathcal{L} . Thus we are not investigating the asymptotic performance of \hat{Y}_S as either $N \rightarrow \infty$ or $|\mathcal{L}| \rightarrow \infty$. With infinite training data, a tree could be made arbitrarily deep, leading to arbitrarily high classification rates since nonparametric classifiers are generally strongly consistent.

Let $E_c \bar{\mu} = (E_c \bar{\mu}(1), \dots, E_c \bar{\mu}(K))$ denote the mean of $\bar{\mu}$ conditioned on $Y = c$: $E_c \bar{\mu}(d) = \frac{1}{N} \sum_{i=1}^N E(\mu_{T_n}(d) | Y = c)$. We make three assumptions about the mean vector, all of which turn out to be true in practice:

1. $\arg \max_d E_c \bar{\mu}(d) = c$.
2. $E_c \bar{\mu}(c) = \alpha_c \gg 1/K$.
3. $E_c \bar{\mu}(d) \sim (1 - \alpha_c)/(K - 1)$.

The validity of the first two is clear from Table 3. The last assumption says that the amount of mass in the mean aggregate distribution that is off the true class tends to be uniformly distributed over the other classes.

Let S_K denote the K -dimensional simplex (probability vectors in \mathbf{R}^K), and let $U_c = \{\mu : \arg \max_d \mu(d) = c\}$, an open convex subset of S_K . Define ϕ_c to be the (Euclidean) distance from $E_c \bar{\mu}$ to ∂U_c , the boundary of U_c . Clearly $\|\mu - E_c \bar{\mu}\| < \phi_c$ implies that $\arg \max_d \mu(d) = c$, where $\|\cdot\|$ denotes Euclidean norm. This is used below to bound the misclassification rate. First, however,

Table 3: Estimates of α_c , γ_c , and e_c for Ten Classes.

Class	0	1	2	3	4	5	6	7	8	9
α_c	0.66	0.86	0.80	0.74	0.74	0.64	0.56	0.86	0.49	0.68
γ_c	0.03	0.01	0.01	0.01	0.03	0.02	0.04	0.01	0.02	0.01
e_c	0.14	0.04	0.03	0.04	0.11	0.13	0.32	0.02	0.23	0.05

we need to compute ϕ_c . Clearly,

$$\partial U_c = \cup_{d, d \neq c} \{\mu \in S_K : \mu(c) = \mu(d)\}.$$

From symmetry arguments, a point in ∂U_c that achieves the minimum distance to $E_c \bar{\mu}$ will lie in each of the sets in the union above. A straightforward computation involving orthogonal projections then yields $\phi_c = (\alpha_c K - 1) / \sqrt{2(K - 1)}$.

Using Chebyshev's inequality, a crude upper bound on the misclassification rate for class c is obtained as follows:

$$\begin{aligned} P(\hat{Y}_S \neq c | Y = c) &= P(\mathbf{x} : \arg \max_d \bar{\mu}(\mathbf{x}, d) \neq c | Y = c) \\ &\leq P(\|\bar{\mu} - E_c \bar{\mu}\| > \phi_c | Y = c) \\ &\leq \frac{1}{\phi_c^2} E \|\bar{\mu} - E_c \bar{\mu}\|^2 \\ &= \frac{1}{\phi_c^2 N^2} \sum_{d=1}^K \left[\sum_{n=1}^N \text{Var}(\mu_{T_n}(d) | Y = c) \right. \\ &\quad \left. + \sum_{n \neq m} \text{Cov}(\mu_{T_n}(d), \mu_{T_m}(d) | Y = c) \right]. \end{aligned}$$

Let η_c denote the sum of the conditional variances, and let γ_c denote the sum of the conditional covariances, both averaged over the trees:

$$\begin{aligned} \frac{1}{N} \sum_{n=1}^N \sum_{d=1}^K \text{Var}(\mu_{T_n}(d) | Y = c) &= \eta_c \\ \frac{1}{N^2} \sum_{n \neq m} \sum_{d=1}^K \text{Cov}(\mu_{T_n}(d), \mu_{T_m}(d) | Y = c) &= \gamma_c. \end{aligned}$$

We see that

$$P(\hat{Y}_S \neq c | Y = c) \leq \frac{\gamma_c + \eta_c / N}{\phi_c^2} = \frac{2(\gamma_c + \eta_c / N)(K - 1)^2}{(\alpha_c K - 1)^2}.$$

Since η_c/N will be small compared with γ_c , the key parameters are α_c and γ_c . This inequality yields only coarse bounds. However, it is clear that under the assumptions above, high classification rates are feasible as long as γ_c is sufficiently small and α_c is sufficiently large, even if the estimates μ_{T_n} are poor.

Observe that the N trees form a simple random sample from some large population \mathcal{T} of trees under a suitable distribution on \mathcal{T} . This is due to the randomization aspect of tree construction. (Recall that at each node, the splitting rule is chosen from a small random sample of queries.) Both $E_c \bar{\mu}$ and the sum of variances are sample means of functionals on \mathcal{T} . The sum of the covariances has the form of a U statistic. Since the trees are drawn independently and the range of the corresponding variables is very small (typically less than 1), standard statistical arguments imply that these sample means are close to the corresponding population means for a moderate number N of trees, say, tens or hundreds. In other words, $\alpha_c \sim E_{\mathcal{T}} E_{\mathbf{X}}(\mu_{\mathcal{T}}(c) | Y = c)$ and $\gamma_c \sim E_{\mathcal{T} \times \mathcal{T}} \sum_{d=1}^K \text{Cov}_{\mathbf{X}}(\mu_{T_1}(d), \mu_{T_2}(d) | Y = c)$. Thus the conditions on α_c and γ_c translate into conditions on the corresponding expectations over \mathcal{T} , and the performance variability among the trees can be ignored.

Table 3 shows some estimates of α_c and γ_c and the resulting bound e_c on the misclassification rate $P(\hat{Y}_S \neq c | Y = c)$. Ten pairs of random trees were made on ten classes to estimate γ_c and α_c . Again, the bounds are crude; they could be refined by considering higher-order joint moments of the trees.

8 Generalization

For convenience, we will consider two types of generalization, referred to as interpolation and extrapolation. Our use of these terms may not be standard and is decidedly ad hoc. Interpolation is the easier case; both the training and testing samples are randomly drawn from (\mathbf{X}, P) , and the number of training samples is sufficiently large to cover the space \mathbf{X} . Consequently, for most test points, the classifier is being asked to interpolate among nearby training points.

By extrapolation we mean situations in which the training samples do not represent the space from which the test samples are drawn—for example, training on a very small number of samples per symbol (e.g., one); using different perturbation models to generate the training and test sets, perhaps adding more severe scaling or skewing; or degrading the test images with correlated noise or lowering the resolution. Another example of this occurred at the first NIST competition (Wilkinson et al., 1992); the hand-printed digits in the test set were written by a different population from those in the distributed training set. (Not surprisingly, the distinguishing feature of the winning algorithm was the size and diversity of the actual samples used to train the classifier.) One way to characterize such situations is to regard P as a mixture distribution $P = \sum_i \alpha_i P_i$, where the P_i might correspond to writer

Table 4: Classification Rates for Various Training Sample Sizes Compared with Nearest-Neighbor Methods.

Sample Size	Trees	$NN(\mathbf{B})$	$NN(\text{raw})$
1	44%	11%	5%
8	87	57	31
32	96	74	55

populations, perturbation models, or levels of degradation, for instance. In complex visual recognition problems, the number of terms might be very large, but the training samples might be drawn from relatively few of the P_i and hence represent a biased sample from P .

In order to gauge the difficulty of the problem, we shall consider the performance of two other classifiers, based on k -nearest-neighbor classification with $k = 5$, which was more or less optimal in our setting. (Using nearest-neighbors as a benchmark is common; see, for example, Geman et al., 1992; Khotanzad & Lu, 1991.) Let $NN(\text{raw})$ refer to nearest-neighbor classification based on Hamming distance in (binary) image space, that is, between bitmaps. This is clearly the wrong metric, but it helps to calibrate the difficulty of the problem. Of course, this metric is entirely blind to invariance but is not entirely unreasonable when the symbols nearly fill the bounding box and the degree of perturbation is limited.

Let $NN(\mathbf{B})$ refer to nearest-neighbor classification based on the binary tag arrangements. Thus, two images \mathbf{x} and \mathbf{x}' are compared by evaluating $Q(\mathbf{x})$ and $Q(\mathbf{x}')$ for all $Q \in \mathbf{B}_0 \subset \mathbf{B}$ and computing the Hamming distance between the corresponding binary sequences. \mathbf{B}_0 was chosen as the subset of binary tag arrangements that split \mathbf{X} to within 5 percent of fifty-fifty. There were 1510 such queries out of the 15,376 binary tag arrangements. Due to invariance and other properties, we would expect this metric to work better than Hamming distance in image space, and of course it does (see below).

8.1 Interpolation. One hundred (randomized) trees were constructed from a training data set with thirty-two samples for each of the $K = 293$ symbols. The average classification rate per tree on a test set \mathcal{V} consisting of 100 samples per symbol is 27 percent. However, the performance of the classifier \hat{Y}_S based on 100 trees is 96 percent. This clearly demonstrates the weak dependence among randomized trees (as well as the discriminating power of the queries). With the $NN(\mathbf{B})$ -classifier, the classification rate was 74 percent; with $NN(\text{raw})$, the rate is 55 percent (see Table 4). All of these rates are on the test set.

When the only random perturbations are nonlinear (i.e., no scaling, rotation, or skew), there is not much standardization that can be done to the

Table 5: Classification Rates for Various Perturbations.

Type of Perturbation	Trees	NN(B)	NN(raw)
Original	96%	74%	55%
Upscaling	88	57	0
Downscaling	80	52	0
Spot noise	71	28	57
Clutter	74	27	59



Figure 11: (Top) Upscaling. (Middle) Downscaling. (Bottom) Clutter.

protocol were used in every experiment. Experiments were repeated several times; the variability was negligible.

One direction that appears promising is explicitly introducing different protocols from tree to tree in order to decrease the dependence. One small experiment was carried out in this direction. All the images were subsampled to half the resolution; for example, 32×32 images become 16×16 . A tag tree was made with 4×4 subimages from the subsampled data set, and one hundred trees were grown using the subsampled training set. The

output of these trees was combined with the output of the original trees on the test data. No change in the classification rate was observed for the original test set. For the test set with spot noise, the two sets of trees each had a classification rate of about 72 percent. Combined, however, they yield a rate of 86 percent. Clearly there is a significant potential for improvement in this direction.

9 Incremental Learning and Universal Trees

The parameters $\mu_{n,\tau}(c) = P(Y = c | T_n = \tau)$ can be incrementally updated with new training samples. Given a set of trees, the actual counts from the training set (instead of the normalized distributions) are kept in the terminal nodes τ . When a new labeled sample is obtained, it can be dropped down each of the trees and the corresponding counters incremented. There is no need to keep the image itself.

This separation between tree construction and parameter estimation is crucial. It provides a mechanism for gradually learning to recognize an increasing number of shapes. Trees originally constructed with training samples from a small number of classes can eventually be updated to accommodate new classes; the parameters can be reestimated. In addition, as more data points are observed, the estimates of the terminal distributions can be perpetually refined. Finally, the trees can be further deepened as more data become available. Each terminal node is assigned a randomly chosen list of minimal extensions of the pending arrangement. The answers to these queries are then calculated and stored for each new labeled sample that reaches that node; again there is no need to keep the sample itself. When sufficiently many samples are accumulated, the best query on the list is determined by a simple calculation based on the stored information, and the node can then be split.

The adaptivity to additional classes is illustrated in the following experiment. A set of one hundred trees was grown with training samples from 50 classes randomly chosen from the full set of 293 classes. The trees were grown to depth 10 just as before (see section 8). Using the original training set of thirty-two samples per class for all 293 classes, the terminal distributions were estimated and recorded for each tree. The aggregate classification rate on all 293 classes was about 90 percent, as compared with about 96 percent when the full training set is used for both quantization and parameter estimation. Clearly fifty shapes are sufficient to produce a reasonably sharp quantization of the entire shape space.

As for improving the parameter estimates, recall that the one hundred trees grown with the pure symbols reached 44 percent on the test set. The terminal distributions of these trees were then updated using the original training set of thirty-two samples per symbol. The classification rate on the same test set climbed from 44 percent to 90 percent.

10 Fast Indexing

One problem with recognition paradigms such as “hypothesize and test” is determining which particular hypothesis to test. Indexing into the shape library is therefore a central issue, especially with methods based on matching image data to model data and involving large numbers of shape classes. The standard approach in model-based vision is to flag plausible interpretations by searching for key features or discriminating parts in hierarchical representations.

Indexing efficiency seems to be inversely related to stability with respect to image degradation. Deformable templates are highly robust because they provide a global interpretation for many of the image data. However, a good deal of searching may be necessary to find the right template. The method of invariant features lies at the other extreme of this axis: the indexing is one shot, but there is not much tolerance to distortions of the data.

We have not attempted to formulate this trade-off in a manner susceptible to experimentation. We have noticed, however, that multiple trees appear to offer a reliable mechanism for fast indexing, at least within the framework of this article and in terms of narrowing down the number of possible classes. For example, in the original experiment with 96 percent classification rate, the five highest-ranking classes in the aggregate distribution $\bar{\mu}$ contained the true class in all but four images in a test set of size 1465 (five samples per class). Even with upscaling, for example, the true label was among the top five in 98 percent of the cases. These experiments suggest that very high recognition rates could be obtained with final tests dedicated to ambiguous cases, as determined, for example, by the mode of the $\bar{\mu}$.

11 Handwritten Digit Recognition

The optical character recognition (OCR) problem has many variations, and the literature is immense; one survey is Mori, Suen, and Yamamoto (1992). In the area of handwritten character recognition, perhaps the most difficult problem is the recognition of unconstrained script; zip codes and hand-drawn checks also present a formidable challenge. The problem we consider is off-line recognition of isolated binary digits. Even this special case has attracted enormous attention, including a competition sponsored by the NIST (Wilkinson et al., 1992), and there is still no solution that matches human performance, or even one that is commercially viable except in restricted situations. (For comparisons among methods, see Bottou et al., 1994, and the lucid discussion in Brown et al., 1993.) The best reported rates seem to be those obtained by the AT&T Bell Laboratories: up to 99.3 percent by training and testing on composites of the NIST training and test sets (Bottou et al., 1994).

We present a brief summary of the results of experiments using the tree-based shape quantization method to the NIST database. (For a more detailed

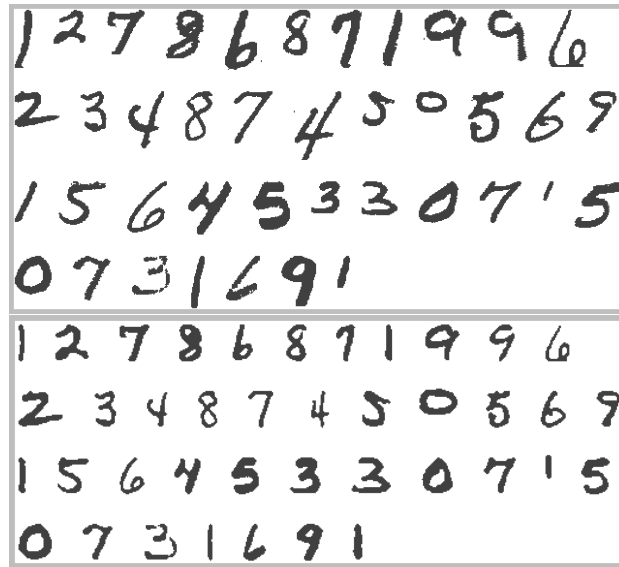


Figure 12: Random sample of test images before (top) and after (bottom) preprocessing.

description, see Geman et al., 1996.) Our experiments were based on portions of the NIST database, which consists of approximately 223,000 binary images of isolated digits written by more than 2000 writers. The images vary widely in dimensions, ranging from about twenty to one hundred rows, and they also vary in stroke thickness and other attributes. We used 100,000 for training and 50,000 for testing. A random sample from the test set is shown in Figure 12.

All results reported in the literature utilize rather sophisticated methods of preprocessing, such as thinning, slant correction, and size normalization. For the sake of comparison, we did several experiments using a crude form of slant correction and scaling, and no thinning. Twenty-five trees were made. We stopped splitting when the number of data points in the second largest class fell below ten. The depth of the terminal nodes (i.e., number of questions asked per tree) varied widely, the average over trees being 8.8. The average number of terminal nodes was about 600, and the average classification rate (determined by taking the mode of the terminal distribution) was about 91 percent. The best error rate we achieved with a single tree was about 7 percent.

The classifier was tested in two ways. First, we preprocessed (scaled and

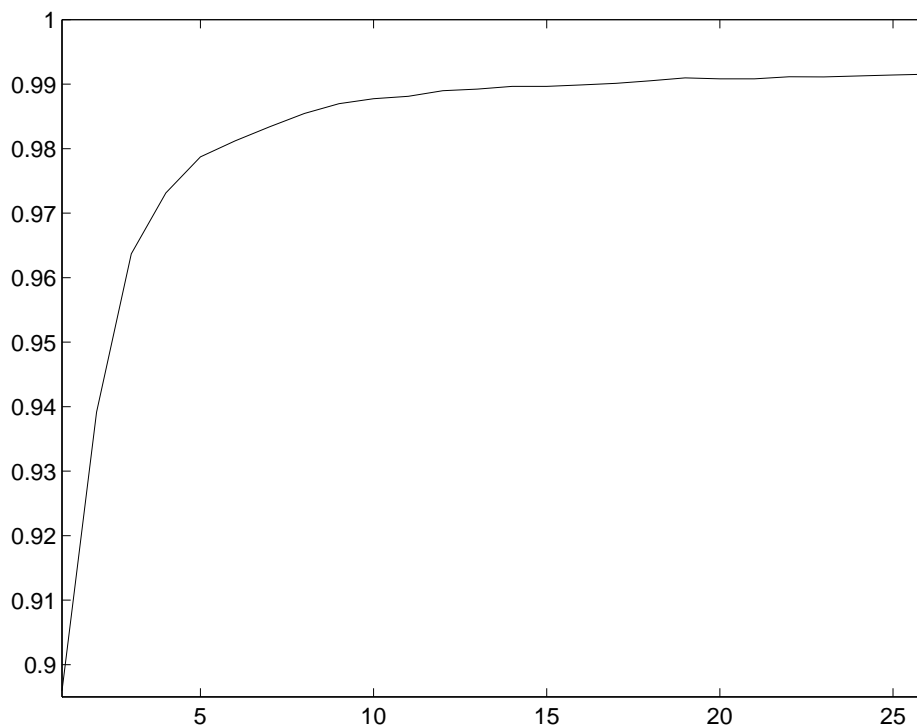


Figure 13: Classification rate versus number of trees.

slant corrected) the test set in the same manner as the training set. The resulting classification rate is 99.2 percent (with no rejection). Figure 13 shows how the classification rate grows with the number of trees. Recall from section 6.1 that the estimated class of an image \mathbf{x} is the mode of the aggregate distribution $\bar{\mu}(\mathbf{x})$. A good measure of the confidence in this estimate is the value of $\bar{\mu}(\mathbf{x})$ at the mode; call it $M(\mathbf{x})$. It provides a natural mechanism for rejection by classifying only those images \mathbf{x} for which $M(\mathbf{x}) > m$; no rejection corresponds to $m = 0$. For example, the classification rate is 99.5 percent with 1 percent rejection and 99.8 percent with 3 percent rejection. Finally, doubling the number of trees makes the classification rates 99.3 percent, 99.6 percent, and 99.8 percent at 0, 1, and 2 percent rejection, respectively.

We performed a second experiment in which the test data were not pre-processed in the manner of the training data; in fact, the test images were classified without utilizing the size of the bounding box. This is especially important in the presence of noise and clutter when it is essentially impossi-

ble to determine the size of the bounding box. Instead, each test image was classified with the same set of trees at two resolutions (original and halved) and three (fixed) slants. The highest of the resulting six modes determines the classification. The classification rate was 98.9 percent.

We classify approximately fifteen digits per second on a single processor SUN Sparcstation 20 (without special efforts to optimize the code); the time is approximately equally divided between transforming to tags and answering questions. Test data can be dropped down the trees in parallel, in which case classification would become approximately twenty-five times faster.

12 Comparison with ANNs

The comparison with ANNs is natural in view of their widespread use in pattern recognition (Werbos, 1991) and several common attributes. In particular, neither approach is model based in the sense of utilizing explicit shape models. In addition, both are computationally very efficient in comparison with model-based methods as well as with memory-based methods (e.g., nearest neighbors). Finally, in both cases performance is diminished by overdedication to the training data (overfitting), and problems result from deficient approximation capacity or parameter estimation, or both. Two key differences are described in the following two subsections.

12.1 The Posterior Distribution and Generalization Error. It is not clear how a feature vector such as \mathbf{Q} could be accommodated in the ANN framework. Direct use is not likely to be successful since ANNs based on very high-dimensional input suffer from poor generalization (Baum & Haussler, 1989), and very large training sets are then necessary in order to approximate complex decision boundaries (Raudys & Jain, 1991).

The role of the posterior distribution $P(Y = c|\mathbf{Q})$ is more explicit in our approach, leading to a somewhat different explanation of the sources of error. In our case, the approximation error results from replacing the entire feature set by an adaptive subset (or really many subsets, one per tree). The difference between the full posterior and the tree-based approximations can be thought of as the analog of approximation error in the analysis of the learning capacity of ANNs (see, e.g., Niyogi & Girosi, 1996). In that case one is interested in the set of functions that can be generated by the family of networks of a fixed architecture. Some work has centered on approximation of the particular function $\mathbf{Q} \rightarrow P(Y = c|\mathbf{Q})$. For example, Lee et al. (1991) consider least-squares approximation to the Bayes rule under conditional independence assumptions on the features; the error vanishes as the number of hidden units goes to infinity.

Estimation error in our case results from an inadequate amount of data to estimate the conditional distributions at the leaves of the trees. The analogous situation for ANNs is well known: even for a network of unlimited

capacity, there is still the problem of estimating the weights from limited data (Niyogi & Girosi, 1996).

Finally, classifiers based on ANNs address classification in a less non-parametric fashion. In contrast to our approach, the classifier has an explicit functional (input-output) representation from the feature vector to \hat{Y} . Of course, a great many parameters may need to be estimated in order to achieve low approximation error, at least for very complex classification problems such as shape recognition. This leads to a relatively large variance component in the bias/variance decomposition. In view of these difficulties, the small error rates achieved by ANNs on handwritten digits and other shape recognition problems are noteworthy.

12.2 Invariance and the Visual System. The structure of ANNs for shape classification is partially motivated by observations about processing in the visual cortex. Thus, the emphasis has been on parallel processing and the local integration (“funneling”) of information from one layer to the next. Since this local integration is done in a spatially stationary manner, translation invariance is achieved. The most successful example in the context of handwritten digit is the convolution neural net LeNET (LeCun et al., 1990). Scale, deformation, and other forms of invariance are achieved to a lesser degree, partially from using gray-level data and soft thresholds, but mainly by utilizing very large training sets and sophisticated image normalization procedures.

The neocognitron (Fukushima & Miyake, 1982; Fukushima & Wake, 1991) is an interesting mechanism to achieve a degree of robustness to shape deformations and scale changes in addition to translation invariance. This is done using hidden layers, which carry out a local ORing operation mimicking the operation of the complex neurons in V1. These layers are referred to as C-type layers in Fukushima and Miyake (1982). A dual-resolution version (Gochin, 1994) is aimed at achieving scale invariance over a larger range.

Spatial stationarity of the connection weights, the C-layers, and the use of multiple resolutions are all forms of ORing aimed at achieving invariance. The complex cell in V1 is indeed the most basic evidence of such an operation in the visual system. There is additional evidence for disjunction at a very global scale in the cells of the inferotemporal cortex with very large receptive fields. These respond to certain shapes at all locations in the receptive field, at a variety of scales but also for a variety of nonlinear deformations such as changes in proportions of certain parts (see Ito, Fujita, Tamura, & Tanaka, 1994; Ito, Tamura, Fujita, & Tanaka, 1995).

It would be extremely inefficient to obtain such invariance through ORing of responses to each of the variations of these shapes. It would be preferable to carry out the global ORing at the level of primitive generic features, which can serve to identify and discriminate between a large class of shapes. We have demonstrated that global features consisting of geometric arrange-

ments of local responses (tags) can do just that. The detection of any of the tag arrangements described in the preceding sections can be viewed as an extensive and global ORing operation. The ideal arrangement, such as a vertical edge northwest of a horizontal edge, is tested at all locations, all scales, and a large range of angles around the northwest vector. A positive response to any of these produces a positive answer to the associated query. This leads to a property we have called semi-invariance and allows our method to perform well without preprocessing and without very large training sets. Good performance extends to transformations or perturbations not encountered during training (e.g., scale changes, spot noise, and clutter).

The local responses we employ are very similar to ones employed at the first level of the convolution neural nets, for example, in Fukushima and Wake (1991). However, at the next level, our geometric arrangements are defined explicitly and designed to accommodate a priori assumptions about shape regularity and variability. In contrast, the features in convolution neural nets are all implicitly derived from local inputs to each layer and from the slack obtained by local ORing, or soft thresholding, carried out layer by layer. It is not clear that this is sufficient to obtain the required level of invariance, nor is it clear how portable they are from one problem to another.

Evidence for correlated activities of neurons with distant receptive fields is accumulating, not only in V1 but in the lateral geniculate nucleus and in the retina (Neuenschwander and Singer, 1996). Gilbert, Das, Ito, Kapadia, and Westheimer (1996) report increasing evidence for more extensive horizontal connections. Large optical point spreads are observed, where subthreshold neural activation appears in an area covering the size of several receptive fields. When an orientation-sensitive cell fires in response to a stimulus in its receptive field, subthreshold activation is observed in cells with the same orientation preference in a wide area outside the receptive field. It appears therefore that the integration mechanisms in V1 are more global and definitely more complex than previously thought. Perhaps the features described in this article can contribute to bridging the gap between existing computational models and new experimental findings regarding the visual system.

13 Conclusion

We have studied a new approach to shape classification and illustrated its performance in high dimensions, with respect to both the number of shape classes and the degree of variability within classes. The basic premise is that shapes can be distinguished from one another by a sufficiently robust and invariant form of recursive partitioning. This quantization of shape space is based on growing binary classification trees using geometric arrangements among local topographic codes as splitting rules. The arrangements are semi-invariant to linear and nonlinear image transformations. As a result,

the method generalizes well to samples not encountered during training. In addition, due to the separation between quantization and estimation, the framework accommodates unsupervised and incremental learning.

The codes are primitive and redundant, and the arrangements involve only simple spatial relationships based on relative angles and distances. It is not necessary to isolate distinguished points along shape boundaries or any other special differential or topological structures, or to perform any form of grouping, matching, or functional optimization. Consequently, a virtually infinite collection of discriminating shape features is generated with elementary computations at the pixel level. Since no classifier based on the full feature set is realizable and since it is impossible to know a priori which features are informative, we have selected features and built trees at the same time by inductive learning. Another data-driven nonparametric method for shape classification is based on ANNs, and a comparison was drawn in terms of invariance and generalization error, leading to the conclusion that prior information plays a relatively greater role in our approach.

We have experimented with the NIST database of handwritten digits and with a synthetic database constructed from linear and nonlinear deformations of about three hundred L^AT_EX symbols. Despite a large degree of within-class variability, the setting is evidently simplified since the images are binary and the shapes are isolated.

Looking ahead, the central question is whether our recognition strategy can be extended to more unconstrained scenarios, involving, for example, multiple or solid objects, general poses, and a variety of image formation models. We are aware that our approach differs from the standard one in computer vision, which emphasizes viewing and object models, 3D matching, and advanced geometry. Nonetheless, we are currently modifying the strategy in this article in order to recognize 3D objects against structured backgrounds (e.g., cluttered desktops) based on gray-level images acquired from ordinary video cameras (see Jedynak & Fleuret, 1996). We are also looking at applications to face detection and recognition.

Acknowledgments

We thank Ken Wilder for many valuable suggestions and for carrying out the experiments on handwritten digit recognition. Yali Amit has been supported in part by the ARO under grant DAAL-03-92-0322. Donald Geman has been supported in part by the NSF under grant DMS-9217655, ONR under contract N00014-91-J-1021, and ARPA under contract MDA972-93-1-0012.

References

- Baum, E. B., & Haussler, D. (1989). What size net gives valid generalization? *Neural Comp.*, 1, 151–160.

- Binford, T. O., & Levitt, T. S. (1993). Quasi-invariants: Theory and exploitation. In *Proceedings of the Image Understanding Workshop* (pp. 819–828). Washington D.C.
- Bottou, L., Cortes, C., Denker, J. S., Drucker, H., Guyon, I., Jackel, L. D., LeCun, Y., Muller, U. A., Sackinger, E., Simard, P., & Vapnik, V. (1994). Comparison of classifier methods: A case study in handwritten digit recognition. *Proc. 12th Inter. Conf. on Pattern Recognition* (Vol. 2, pp. 77–82). Los Alamitos, CA: IEEE Computer Society Press.
- Breiman, L. (1994). *Bagging predictors* (Tech. Rep. No. 451). Berkeley: Department of Statistics, University of California, Berkeley.
- Breiman, L., Friedman, J., Olshen, R., & Stone, C. (1984). *Classification and regression trees*. Belmont, CA: Wadsworth.
- Brown, D., Corruble, V., & Pittard, C. L. (1993). A comparison of decision tree classifiers with backpropagation neural networks for multimodal classification problems. *Pattern Recognition*, 26, 953–961.
- Burns, J. B., Weiss, R. S., & Riseman, E. M. (1993). View variation of point set and line segment features. *IEEE Trans. PAMI*, 15, 51–68.
- Casey, R. G., & Jih, C. R. (1983). A processor-based OCR system. *IBM Journal of Research and Development*, 27, 386–399.
- Casey, R. G., & Nagy, G. (1984). Decision tree design using a probabilistic model. *IEEE Trans. Information Theory*, 30, 93–99.
- Cover, T. M., & Thomas, J. A. (1991). *Elements of information theory*. New York: Wiley.
- Dietterich, T. G., & Bakiri, G. (1995). Solving multiclass learning problems via error-correcting output codes. *J. Artificial Intell. Res.*, 2, 263–286.
- Forsyth, D., Mundy, J. L., Zisserman, A., Coelho, C., Heller, A., & Rothwell, C. (1991). Invariant descriptors for 3-D object recognition and pose. *IEEE Trans. PAMI*, 13, 971–991.
- Friedman, J. H. (1973). A recursive partitioning decision rule for nonparametric classification. *IEEE Trans. Comput.*, 26, 404–408.
- Fukushima, K., & Miyake, S. (1982). Neocognitron: A new algorithm for pattern recognition tolerant of deformations and shifts in position. *Pattern Recognition*, 15, 455–469.
- Fukushima, K., & Wake, N. (1991). Handwritten alphanumeric character recognition by the neocognitron. *IEEE Trans. Neural Networks*, 2, 355–365.
- Gelfand, S. B., & Delp, E. J. (1991). On tree structured classifiers. In I. K. Sethi & A. K. Jain (Eds.), *Artificial neural networks and statistical pattern recognition* (pp. 51–70). Amsterdam: North-Holland.
- Geman, D., Amit, Y., & Wilder, K. (1996). *Joint induction of shape features and tree classifiers* (Tech. Rep.). Amherst: University of Massachusetts.
- Geman, S., Bienenstock, E., & Doursat, R. (1992). Neural networks and the bias/variance dilemma. *Neural Computation*, 4, 1–58.
- Gilbert, C. D., Das, A., Ito, M., Kapadia, M., & Westheimer, G. (1996). Spatial integration and cortical dynamics. *Proc. Natl. Acad. Sci.*, 93, 615–622.
- Gochin, P. M. (1994). Properties of simulated neurons from a model of primate inferior temporal cortex. *Cerebral Cortex*, 5, 532–543.
- Guo, H., & Gelfand, S. B. (1992). Classification trees with neural network feature

- extraction. *IEEE Trans. Neural Networks*, 3, 923–933.
- Hastie, T., Buja, A., & Tibshirani, R. (1995). Penalized discriminant analysis. *Annals of Statistics*, 23, 73–103.
- Hussain, B., & Kabuka, M. R. (1994). A novel feature recognition neural network and its application to character recognition. *IEEE Trans. PAMI*, 16, 99–106.
- Ito, M., Fujita, I., Tamura, H., Tanaka, K. (1994). Processing of contrast polarity of visual images of inferotemporal cortex of Macaque monkey. *Cerebral Cortex*, 5, 499–508.
- Ito, M., Tamura, H., Fujita, I., & Tanaka, K. (1995). Size and position invariance of neuronal response in monkey inferotemporal cortex. *J. Neuroscience*, 73(1), 218–226.
- Jedynak, B., Fleuret, F. (1996). Reconnaissance d'objets 3D à l'aide d'arbres de classification. In *Proc. Image Com 96*. Bordeaux, France.
- Jung, D.-M., & Nagy, G. (1995). Joint feature and classifier design for OCR. In *Proc. 3rd Inter. Conf. Document Analysis and Processing* (Vol. 2, pp. 1115–1118). Montreal. Los Alamitos, CA: IEEE Computer Society Press.
- Khotanzad, A., & Lu, J.-H. (1991). Shape and texture recognition by a neural network. In I. K. Sethi & A. K. Jain (Eds.), *Artificial Neural Networks and Statistical Pattern Recognition*. Amsterdam: North-Holland.
- Knerr, S., Personnaz, L., & Dreyfus, G. (1992). Handwritten digit recognition by neural networks with single-layer training. *IEEE Trans. Neural Networks*, 3, 962–968.
- Kong, E. B., & Dietterich, T. G. (1995). Error-correcting output coding corrects bias and variance. In *Proc. of the 12th International Conference on Machine Learning* (pp. 313–321). San Mateo, CA: Morgan Kaufmann.
- Lamdan, Y., Schwartz, J. T., & Wolfson, H. J. (1988). Object recognition by affine invariant matching. In *IEEE Int. Conf. Computer Vision and Pattern Rec.* (pp. 335–344). Los Alamitos, CA: IEEE Computer Society Press.
- LeCun, Y., Boser, B., Denker, J. S., Henderson, D., Howard, R. E., Hubbard, W., & Jackel, L. D. (1990). Handwritten digit recognition with a back-propagation network. In D. S. Touretzky (Ed.), *Advances in Neural Information* (Vol. 2). San Mateo, CA: Morgan Kaufmann.
- Lee, D.-S., Srihari, S. N., & Gaborski, R. (1991). Bayesian and neural network pattern recognition: A theoretical connection and empirical results with handwritten characters. In I. K. Sethi & A. K. Jain (Eds.), *Artificial Neural Networks and Statistical Pattern Recognition*. Amsterdam: North-Holland.
- Martin, G. L., & Pitman, J. A. (1991). Recognizing hand-printed letters and digits using backpropagation learning. *Neural Computation*, 3, 258–267.
- Mori, S., Suen, C. Y., & Yamamoto, K. (1992). Historical review of OCR research and development. In *Proc. IEEE* (Vol. 80, pp. 1029–1057). New York: IEEE.
- Mundy, J. L., & Zisserman, A. (1992). *Geometric invariance in computer vision*. Cambridge, MA: MIT Press.
- Neuenschwander, S., & Singer, W. (1996). Long-range synchronization of oscillatory light responses in cat retina and lateral geniculate nucleus. *Nature*, 379(22), 728–733.

- Niyogi, P., & Girosi, F. (1996). On the relationship between generalization error, hypothesis complexity, and sample complexity for radial basis functions. *Neural Comp.*, *8*, 819–842.
- Quinlan, J. R. (1986). Induction of decision trees. *Machine Learning*, *1*, 81–106.
- Raudys, S., & Jain, A. K. (1991). Small sample size problems in designing artificial neural networks. In I. K. Sethi & A. K. Jain (Eds.), *Artificial Neural Networks and Statistical Pattern Recognition*. Amsterdam: North-Holland.
- Reiss, T. H. (1993). *Recognizing planar objects using invariant image features*. Lecture Notes in Computer Science no. 676. Berlin: Springer-Verlag.
- Sabourin, M., & Mitiche, A. (1992). Optical character recognition by a neural network. *Neural Networks*, *5*, 843–852.
- Sethi, I. K. (1991). Decision tree performance enhancement using an artificial neural network implementation. In I. K. Sethi & A. K. Jain (Eds.), *Artificial Neural Networks and Statistical Pattern Recognition*. Amsterdam: North-Holland.
- Shlien, S. (1990). Multiple binary decision tree classifiers. *Pattern Recognition*, *23*, 757–763.
- Simard, P. Y., LeCun, Y. L., & Denker, J. S. (1994). Memory-based character recognition using a transformation invariant metric. In *Proc. 12th Inter. Conf. on Pattern Recognition* (Vol. 2, pp. 262–267). Los Alamitos, CA: IEEE Computer Society Press.
- Werbos, P. (1991). Links between artificial neural networks (ANN) and statistical pattern recognition. In I. K. Sethi & A. K. Jain (Eds.), *Artificial Neural Networks and Statistical Pattern Recognition*. Amsterdam: North-Holland.
- Wilkinson, R. A., Geist, J., Janet, S., Grother, P., Gurses, C., Creecy, R., Hammond, B., Hull, J., Larsen, N., Vogl, T., & and Wilson, C. (1992). *The first census optical character recognition system conference* (Tech. Rep. No. NISTIR 4912). Gaithersburg, MD: National Institute of Standards and Technology.

Received April 18, 1996; accepted November 1, 1996.